ACS OMEGA

http://pubs.acs.org/journal/acsodf

Article

Ultrasound-Assisted Synthesis of a ZnO/$BiVO_4$ S-Scheme Heterojunction Photocatalyst for Degradation of the Reactive Red 141 Dye and Oxytetracycline Antibiotic

Khemika Wannakan, Kamonpan Khansamrit, Teeradech Senasu, and Suwat Nanan*

Cite This: *ACS Omega* 2023, 8, 4835−4852

Read Online

ACCESS | Metrics & More | Article Recommendations

ABSTRACT: The preparation of novel sunlight active photocatalysts for complete removal of pollutants from aqueous solutions is a vital research topic in environmental protection. The present work reports the synthesis of a ZnO/$BiVO_4$ S-scheme heterojunction photocatalyst for degradation of the reactive red dye and oxytetracycline antibiotic in wastewater. ZnO and $BiVO_4$ were first fabricated by a hydrothermal technique, and then, the ZnO/$BiVO_4$ heterostructure was synthesized using an ultrasonic route. An increase of the surface area, compared to that of ZnO, was found in ZnO/$BiVO_4$. The enhancement of charge separation efficiency at the interface was obtained so that a remarkable enhancement of the photocatalytic performance was detected in the prepared heterojunction photocatalyst. Complete detoxification of harmful pollutants was achieved by using the economical solar energy. The removal of the pollutants follows the first-order reaction with the highest rate constant of 0.107 min^{-1}. The stability of the prepared photocatalyst was detected after five cycles of use. The ZnO/$BiVO_4$ S-scheme heterostructure photocatalyst still provides high photoactivity even after five times of use. Hydroxyl radicals play an important role in the removal of the pollutant. This work demonstrates a new route to create the step-scheme heterojunction with high photoactivity for complete removal of the toxic dye and antibiotic in the environment.

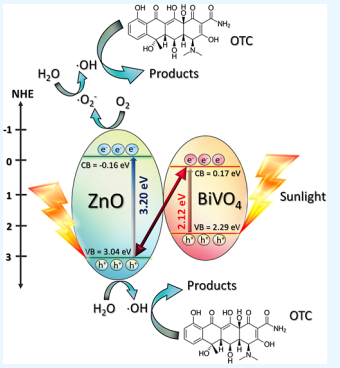

1. INTRODUCTION

A large variety of harmful dyes have been found in toxic wastewater effluents from various industries including textile and pharmaceutical sectors.[1−5] Reactive dyes are basically classified by the presence of azo chromophores, which are considered toxic and mutagenic to living organisms.[6−9] A very small amount of the reactive red azo dye in water is visible and undesirable.[10] Thus, it is a matter of high concern to find out a cost-effective technology for the treatment of water containing this toxic dye.[10,11] The oxytetracycline (OTC) antibiotic is extensively used in humans for the treatment of bacterial infectious diseases.[12−15] However, this drug causes a serious problem to the environment. After OTC is metabolized in the body, there is a chance that the toxic byproducts could enter the natural water.[16,17] This causes damage to the ecosystem and human health. Therefore, complete removal of the toxic organic contaminants from the aqueous phase is urgently needed.[18−22]

Several techniques including adsorption were used to treat the pollutants in wastewater. However, the incomplete removal of the contaminants and the generation of secondary pollutants are the main drawbacks of these conventional methods.[23−25] Interestingly, a semiconducting photocatalytic route is a promising technique for complete removal of the toxic organic pollutants.[5,16,17] Basically, the commercially available TiO_2 is a UV-active photocatalyst with low photoactivity under natural sunlight.[26−31] The ZnO photocatalyst has gained much attention because it shows excellent transport property, is inexpensive, and has a versatile morphology.[32−34] In addition, based on our previous studies, controlled synthesis can be performed very easily for the creation of ZnO with high performance and also with a low cost of production.[1,3,5−7] Therefore, in comparison to TiO_2, ZnO is much cheaper and very easy to synthesize controllably. Nevertheless, low sunlight performance and occurrence of the photocorrosion are the main drawbacks influencing the practical application of ZnO.[35] Alternatively, preparation of the visible-light-responsive photocatalysts is one of the most promising research topics in the field of photocatalysis due to the advantage of complete degradation of the toxic pollutants by the utilization of abundant solar energy.[36−39]

Sunlight active photocatalysts including bismuth vanadate ($BiVO_4$) have gained much attention. Monoclinic $BiVO_4$ comprising an Aurivillius structure shows the advantages of non-toxicity, excellent structural stability, and good visible light

Received: October 31, 2022
Accepted: January 19, 2023
Published: January 26, 2023

https://doi.org/10.1021/acsomega.2c07020
ACS Omega 2023, 8, 4835−4852

response.[40−45] However, this pristine photocatalyst faces the problem of a high electron−hole recombination rate and severe photocorrosion after photodegradation study.[46−48] In theory, doping of noble metals or fabrication of the semiconducting heterojunctions are the two main strategies for the improvement of the resultant photocatalytic performance.[49−54] However, utilization of gold or silver metals is quite expensive. Therefore, generation of a heterojunction is a promising alternative method to create the new photocatalyst with high performance. According to the literature, some heterojunctions based on $BiVO_4$ have been reported.[55−57]

After the coupling of ZnO and $BiVO_4$, an improvement of electron−hole separation efficiency is expected. This will end up with an enhancement of the resultant photocatalytic performance. On examining the ZnO/$BiVO_4$ heterojunction, it is noted that many techniques have been used for the preparation of the ZnO/$BiVO_4$ binary composite.[36−38,41,43,45−47] Among these various methods, ultrasonication is one of the most popular techniques for the creation of the photocatalyst heterojunction. This is due to the advantages of low cost, low energy consumption, and easy control.[58−64]

To study a heterojunction semiconductor, fabrication of a new heterostructure photocatalyst by coupling of two photocatalysts was introduced. It is well-known that both type II and Z-scheme heterojunctions have previously been proposed.[65,66] However, the electron transfer mechanism of a conventional Z-scheme photocatalyst faces some drawbacks so that the new model based on a step scheme or S-scheme photocatalyst with excellent charge separation and high redox ability was introduced. In principle, the advantages of extended photoabsorption, excellent charge separation, and strong redox potential are obtained.[65−68]

From the above discussion, the present work aims to create a ZnO/$BiVO_4$ S-scheme heterostructure photocatalyst for the degradation of the dye and antibiotic by the utilization of abundant solar energy. Bare ZnO and pristine $BiVO_4$ were prepared first by a facile hydrothermal method. Subsequently, the ZnO/$BiVO_4$ S-scheme photocatalyst was then synthesized using an ultrasonic route. An improvement of the surface area, compared to that of bare ZnO, and a dramatic lowering of the electron−hole recombination rate at the interface are the two key factors concerning the remarkable enhancement of the photocatalytic performance detected in the prepared ZnO/$BiVO_4$ heterojunction photocatalyst. Complete removal of toxic pollutants under sunlight was obtained. The excellent stability of the photocatalyst, with high photoactivity, was confirmed after five times of use. Hydroxyl radicals play a major role in the pollutant removal, while photogenerated holes and electrons play a minor role. Charge transfer at the interface belongs to the S-scheme heterojunction. The novelty of the work is based on the use of an ultrasonic route to create the S-scheme ZnO/$BiVO_4$ heterostructure photocatalyst for the removal of the OTC antibiotic. This type of heterojunction thermodynamically favors photocatalytic reactions due to the huge driving force provided by its strong redox abilities. This work offers a novel avenue to fabricate the heterostructure photocatalyst with high photoactivity for complete detoxification of the harmful dye and antibiotic in natural water.

2. EXPERIMENT

2.1. Chemicals and Reagents. All chemicals were used as received. Ultrapure water [deionized (DI) water, 18.2 MΩ·cm^{-1}] was used.

2.2. Synthesis of $BiVO_4$. The bismuth vanadate ($BiVO_4$) catalyst was prepared by a hydrothermal method.[16] First, solution A was prepared by the dispersion of 2.4238 g of $Bi(NO_3)_3{\cdot}5H_2O$ in 30 cm^3 of 1.5 M HNO_3. Second, solution B was obtained by the addition of 0.5849 g of NH_4VO_3 and 1.2656 g of ethylenediaminetetraacetic acid (EDTA) in 30 cm^3 of DI water. Third, solution B was added to solution A, and the pH of the mixture was adjusted to reach about 7 by the addition of NaOH solution. It was then transferred into a 100 cm^3 Teflon-lined autoclave, which maintains the temperature of 100 °C for 24 h. After that, the precipitate was collected, washed with water and ethanol, and finally dried at 60 °C for 15 h.

2.3. Synthesis of ZnO. The zinc oxide (ZnO) photocatalyst was also fabricated via a hydrothermal route as well.[5] The Zn^{2+} solution was prepared by dissolving 3.6100 g of $Zn(CH_3COO)_2{\cdot}2H_2O$ in 30 cm^3 of DI water. Meanwhile, the OH^- solution was separately prepared by dissolving 3.2900 g of NaOH in 30 cm^3 of DI water. The OH^- solution was then added dropwise to the Zn^{2+} solution with continuous stirring for 30 min. The reaction mixture was transferred into an autoclave that maintains the temperature of 150 °C for 24 h. The resultant precipitate was collected, washed with water and ethanol, and finally dried at 80 °C for 15 h.

2.4. Synthesis of ZnO/$BiVO_4$. ZnO/$BiVO_4$ was fabricated by an ultrasonic route. In a typical procedure, about 0.2 g of ZnO was dispersed in 10 cm^3 of DI water for 60 min in an ultrasonic bath (dispersion A). Separately, ultrasonication of $BiVO_4$ (0.2 g of the sample in 10 cm^3 of DI water) was also performed for 60 min (dispersion B). Dispersion A was then added into dispersion B, and the mixture was further ultrasonicated for 120 min. Afterward, about 15 cm^3 of acetone was added to the mixture, which was then left for 24 h with continuous stirring. After the centrifugation, the product was collected, washed with water and ethanol, and finally dried at 60 °C for 15 h.

2.5. Characterization. All sample were characterized using the same method described previously.[1,3,5−7] Basically, the structure of the prepared catalyst was recorded by X-ray diffraction (XRD) using a PANalytical EMPYREAN X-ray diffractometer comprising monochromatic Cu Kα radiation. The morphological structure and the element constitution of the samples were examined by field emission scanning electron microscopy (FESEM, FEI Helios NanoLab G3 CX). The transmission electron microscopy (TEM) and high-resolution TEM (HRTEM) images of the photocatalyst were obtained on an FEI TECNAI G2 20. The Fourier transform infrared (FT-IR) spectra were recorded on a PerkinElmer Spectrum One FT-IR spectrophotometer. The sample preparation was performed by a KBr pellet method. The Brunauer−Emmett−Teller (BET) specific surface area and porosity were elucidated by a Micromeritics ASAP 2460 surface area and porosity analyzer. Optical properties were determined through ultraviolet−visible (UV−vis) diffused reflectance spectroscopy (Shimazu UV−VISNIR-3101PC scanning spectrophotometer) and photoluminescence (PL) spectroscopy (Shimazu RF-5301PC).

https://doi.org/10.1021/acsomega.2c07020
ACS Omega 2023, 8, 4835−4852

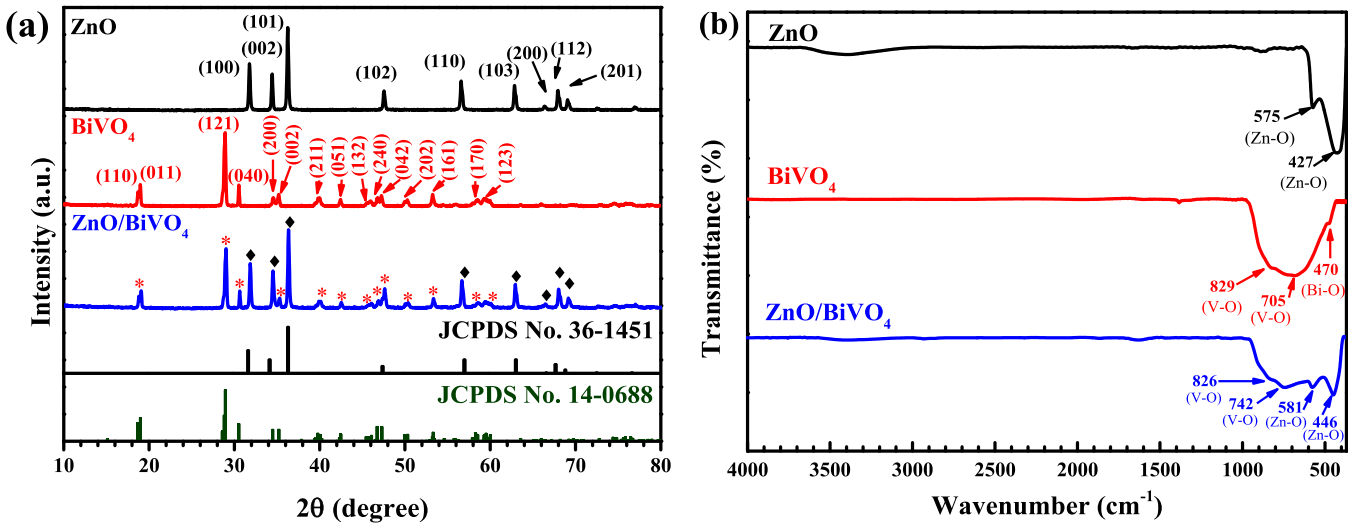

Figure 1. XRD patterns (a) and FT-IR spectra (b) of ZnO, $BiVO_4$, and ZnO/$BiVO_4$ photocatalysts.

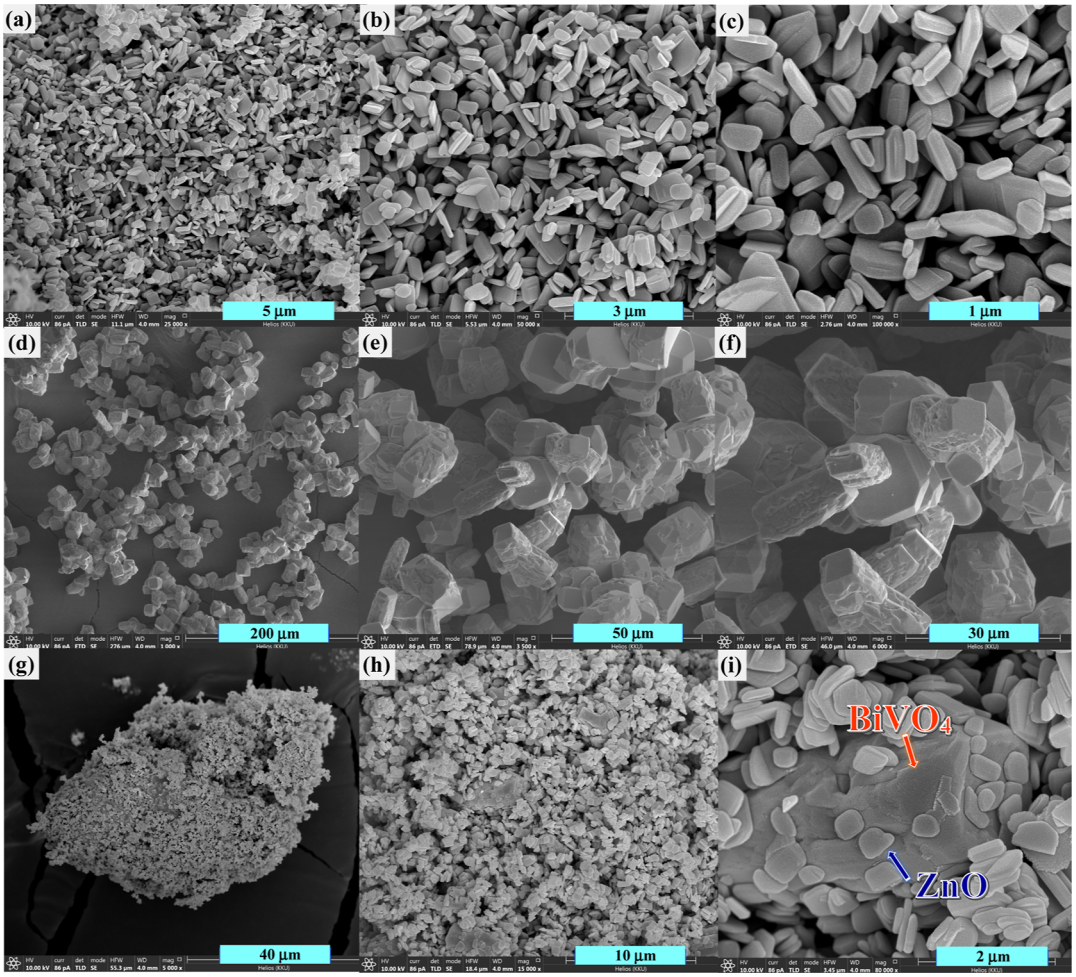

Figure 2. FESEM micrographs of ZnO (a–c), $BiVO_4$ (d–f), and ZnO/$BiVO_4$ photocatalysts (g–i).

2.6. Photocatalytic Degradation of the Pollutants. The photocatalytic performance of all prepared photocatalysts was determined by monitoring the degradation of the OTC antibiotic and RR141 dye under UV light (a mercury lamp, 125 W) and natural sunlight. The details of the photocatalytic study can be found elsewhere.[5,16,17]

Typically, the blank experiment was carried out by irradiating the pollutant solution without the incorporation of the photocatalyst.[16,17] The photocatalytic study was performed in an aqueous solution (200 cm^3) of either the OTC antibiotic or the RR141 dye (concentration = 10 ppm) in the presence of the photocatalyst (50 mg). The solution of 5

https://doi.org/10.1021/acsomega.2c07020
ACS Omega 2023, 8, 4835−4852

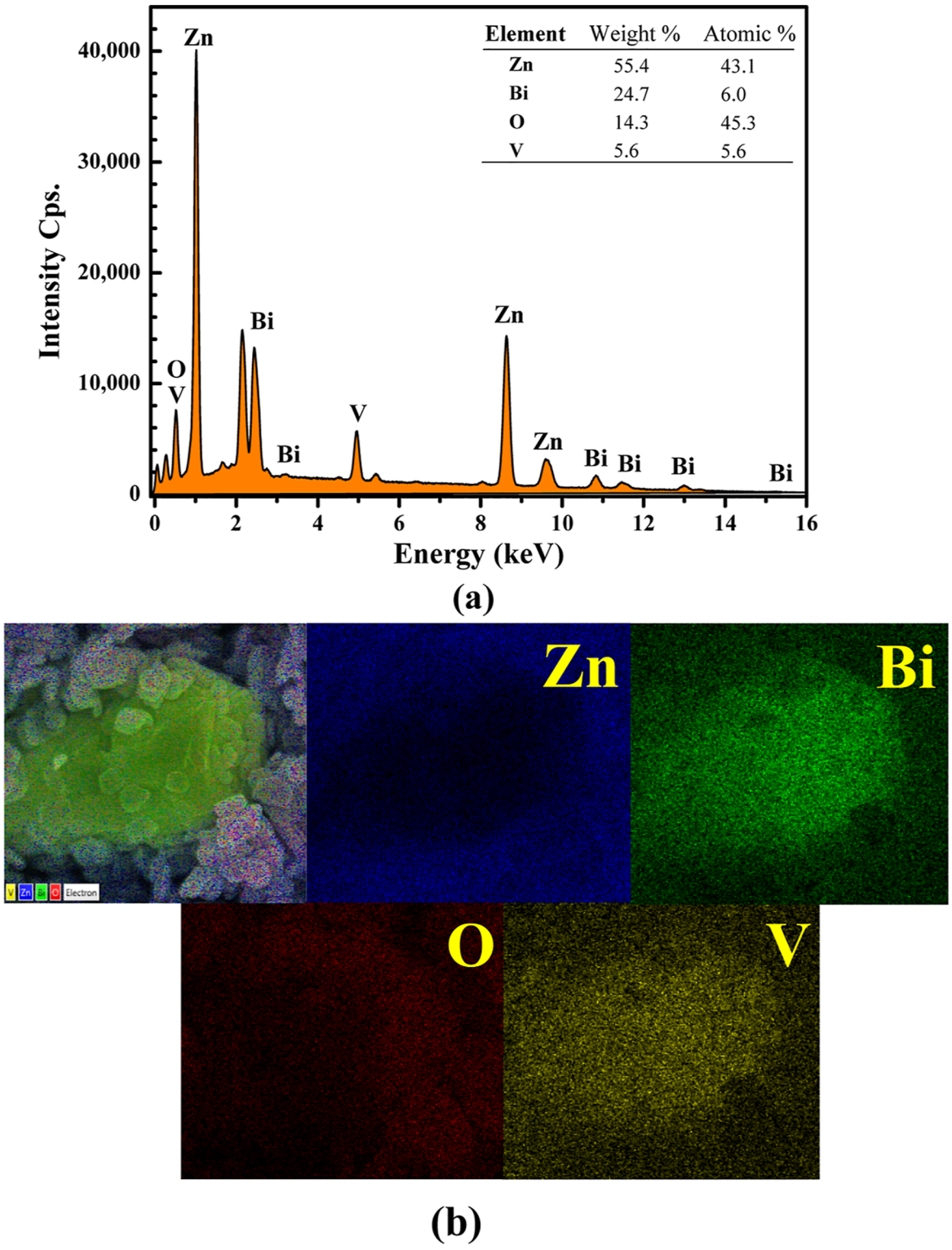

Figure 3. EDS spectrum and SEM image of the mapping area (a) and EDS elementary mapping of Zn O, Bi, and V obtained from the ZnO/$BiVO_4$ photocatalyst (b).

cm^3 was sampled after light irradiation. The exact concentration of either RR141 or OTC was determined at the λ_{max} values of 543 and 354 nm, respectively, by a spectrophotometric method.

The photoactivity toward the degradation of the pollutant was calculated as follows.

$$\text{photoactivity}\ (\%) = (1 - C/C_0) \times 100\% \quad (1)$$

where C_0 and C represent the initial concentration and the concentration of the pollutant solution after different times of photo illumination, respectively.

The performance of the prepared photocatalyst can also be determined from the photocatalytic degradation rate as shown below.

https://doi.org/10.1021/acsomega.2c07020
ACS Omega 2023, 8, 4835−4852

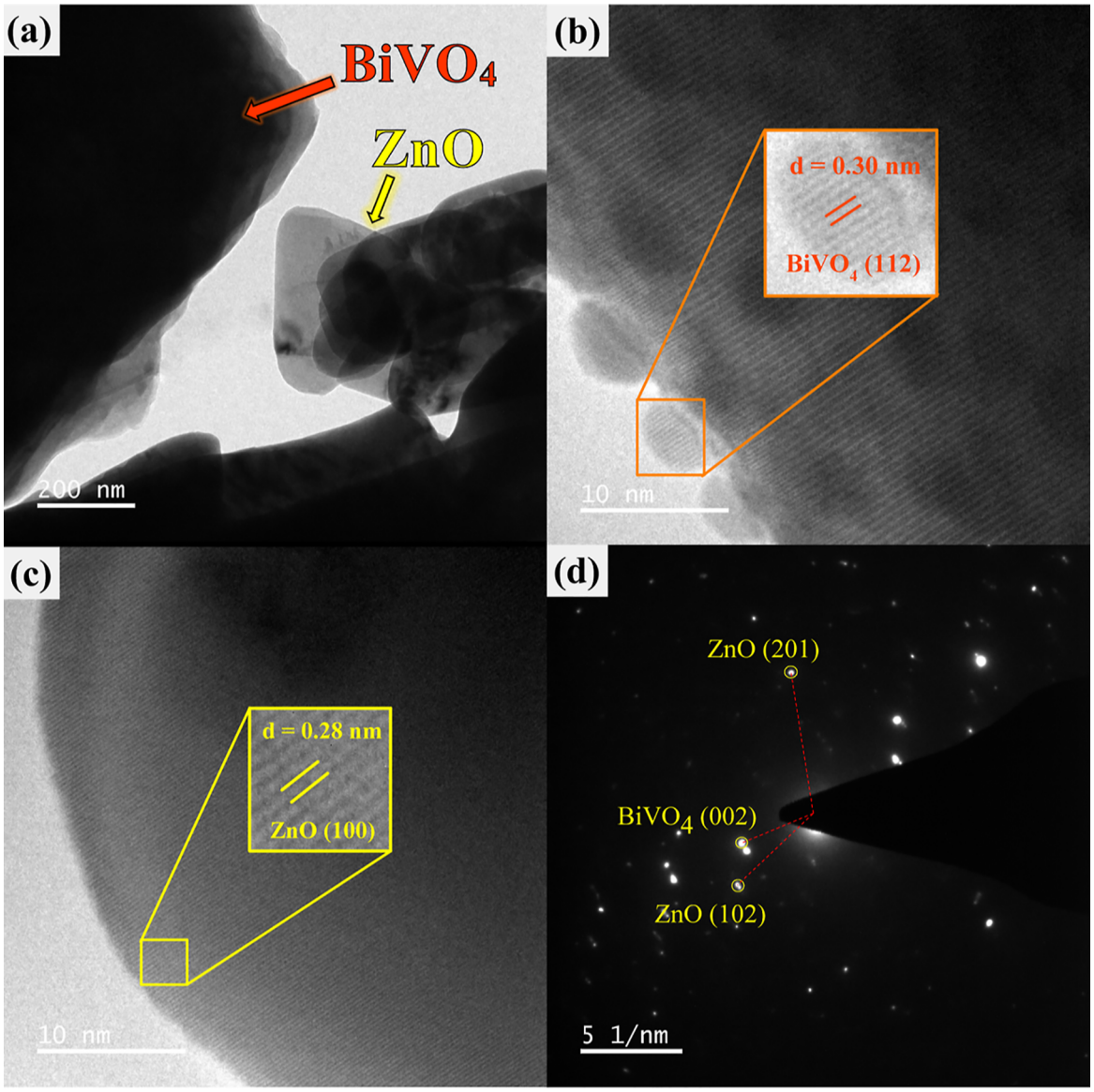

Figure 4. TEM image (a), HR-TEM image (b,c), and SAED pattern (d) obtained from the ZnO/$BiVO_4$ photocatalyst.

$$dC/dt = -k_1 C \quad (2)$$

$$\ln(C_0/C) = k_1 t \quad (3)$$

where k_1 is the rate constant of the first-order degradation reaction.

To study the crucial species involved in the removal of the pollutant, each scavenger (5 mM), namely, isopropyl alcohol (IPA), NaN_3, EDTA-2Na, or $K_2Cr_2O_7$, was separately added for the quenching of hydroxyl radicals, superoxide anion radicals, holes, and electrons, respectively.[3] In addition, KI was also incorporated as a scavenger of surface hydroxyl radicals and holes. Each scavenger was separately incorporated in the presence of the prepared photocatalyst.[5,16,17]

To confirm the generation of the hydroxyl radicals, the photocatalyst was dispersed in terephthalic acid (TA) solution.[17] The formation of the radicals was examined by using a spectrofluorometer (excitation wavelength of 315 nm).

To investigate the reusability of the photocatalyst, the used photocatalyst was filtered, washed with ethanol and water, and then dried before use in the second run.[3,5,17] The reuse of the sample was carried out for five consecutive runs.

3. RESULTS AND DISCUSSION

3.1. Characterization of the Photocatalyst. The XRD patterns of all prepared photocatalyst are shown in Figure 1a. The monoclinic $BiVO_4$ photocatalyst displayed diffraction at 2θ values of 18.67, 19.00, 28.90, 30.50, 34.50, 35.22 39.80, 42.50, 45.84, 46.74, 47.30, 50.30, and 53.20°, assigned to the reflection planes of (110), (011), (121), (040), (200), (002), (211), (051), (213), (240), (042), (202), and (161), respectively. This agrees well the JCPDS no. 14-0688 file.[16,17] The pattern from the XRD diffractogram of bare ZnO belongs to the hexagonal wurtzite structure (JCPDS no. 36-1451).[5] The diffraction located at 2θ values of 31.76, 34.41, 36.25, 47.53, 56.5962.85, 66.37, 67.94, and 69.08° corresponded to the reflection from crystal planes of (100), (002), (101), (102), (110), (103), (200), (112), and (201), respectively. It can be seen that the ZnO/$BiVO_4$ photocatalyst showed the diffraction peaks contributing from both ZnO and

https://doi.org/10.1021/acsomega.2c07020
ACS Omega 2023, 8, 4835−4852

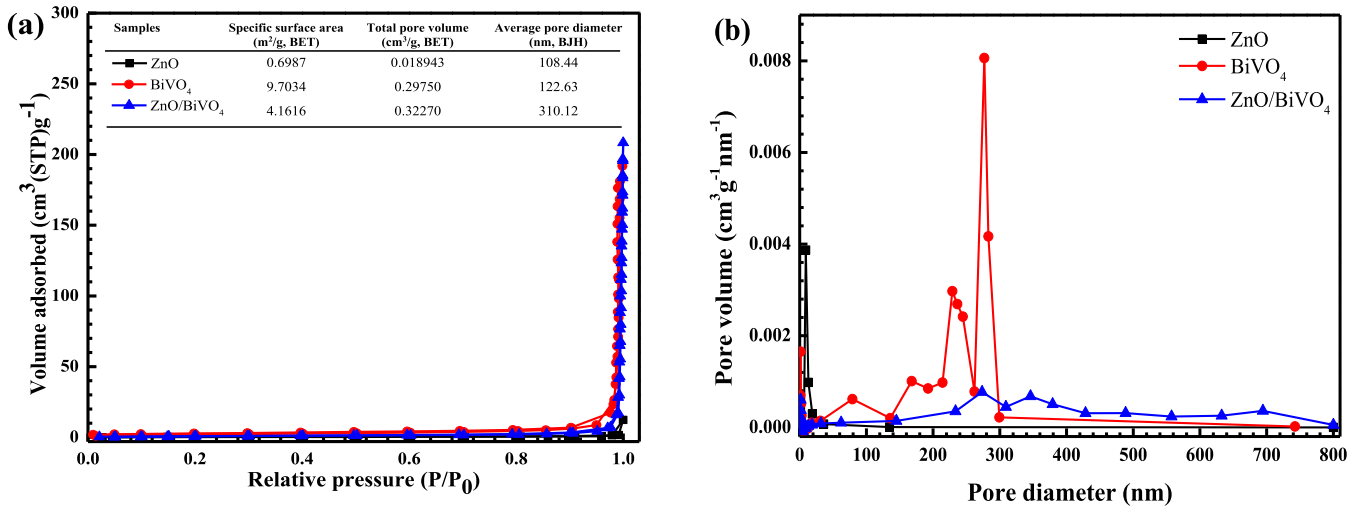

Figure 5. N_2 adsorption−desorption isotherms (a) and pore size distributions (b) of ZnO, $BiVO_4$, and ZnO/$BiVO_4$ photocatalysts.

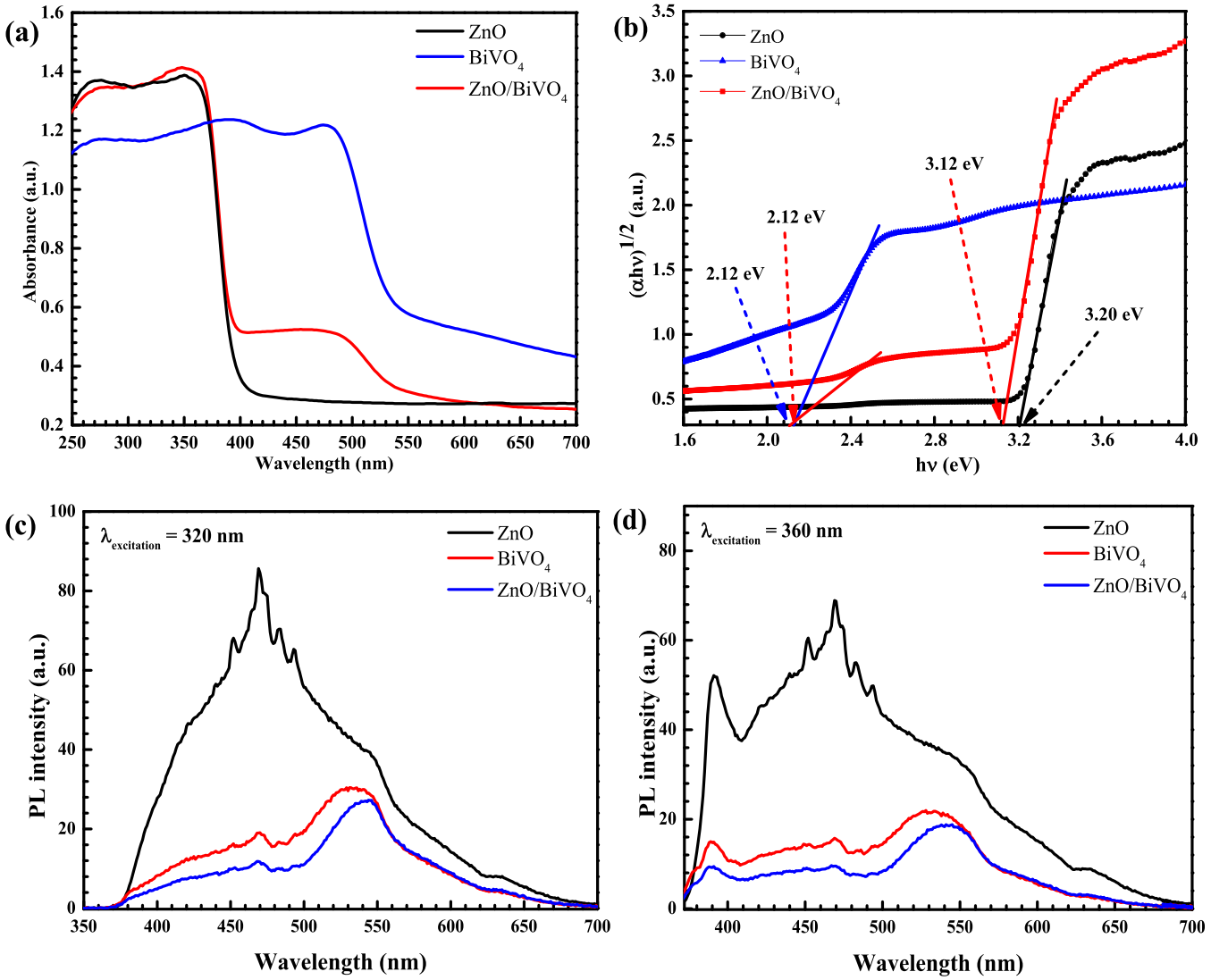

Figure 6. Diffused reflectance spectra (a), Tauc plot for the determination of the band gap (b), and PL spectra of the samples using $\lambda_{excitation}$ values of 320 (c) and 360 nm (d).

$BiVO_4$. The result confirms the successful creation of the heterojunction.

FT-IR spectra of all samples were recorded and are shown in Figure 1b. $BiVO_4$ showed bands at 705 and 829 cm^{-1},

https://doi.org/10.1021/acsomega.2c07020
ACS Omega 2023, 8, 4835−4852

respectively, indicating the ν_3 asymmetric and ν_1 symmetric stretching of VO_4^3. The presence of the peak at 470 cm^{-1} was attributed to the stretching of the Bi−O bond.[16,17] The vibrational peaks at 427 and 575 cm^{-1} were due to stretching vibration from the Zn−O bond.[5] In the case of the ZnO/$BiVO_4$ photocatalyst, the vibrational bands of both the Bi−O bond and Zn−O bond were clearly observed. This confirms the co-existence of both ZnO and $BiVO_4$. The result correlates well with those obtained by XRD.

The morphological structures of ZnO, $BiVO_4$, and ZnO/$BiVO_4$ were elucidated by the scanning electron microscopy (SEM) method. The SEM images of pristine ZnO (Figure 2a−c) showed a thin disk-like morphological structure of about 0.30 μm × 0.50 μm × 0.12 μm dimensions. Meanwhile, the SEM images of the bare $BiVO_4$ photocatalyst (Figure 2d−f) showed an irregular polygon morphology of about 8.84 μm × 8.50 μm dimensions. As seen in Figure 2g−i, the final morphology of ZnO/$BiVO_4$ showed the co-existence of both ZnO and $BiVO_4$ without altering the morphology of the individual photocatalyst.

Energy-dispersive X-ray spectroscopy (EDS) was used to determine the elemental compositions in the sample. Four elements, including Zn, O, Bi, and V, were detected in the synthesized photocatalyst (Figure 3a). The atomic percentages of 43.1, 6.0, 45.3, and 5.6%, were detected for Zn, O, Bi, and V, respectively. The result confirms the element composition in the prepared photocatalyst. Furthermore, the dispersion of all elements was elucidated by EDS elemental mapping (Figure 3b). The uniform distribution of Zn, O, Bi, and V elements was confirmed.

The successful creation of ZnO/$BiVO_4$ was also examined by the TEM method. The TEM image of the heterojunction is shown in Figure 4a. The HR-TEM micrographs in Figure 4b,c showed the interplanar spacings of 0.30 and 0.28 nm, assigned to the existence of the (112) crystal plane of $BiVO_4$ and the (100) plane of ZnO, respectively. The selected area electron diffraction (SAED) pattern (Figure 4d) revealed the monocrystalline nature of the prepared photocatalyst comprising those of ZnO and $BiVO_4$.[5] The results agree well with those from XRD, FT-IR spectroscopy, and EDS−FESEM presented previously. Thus, the co-existence of both ZnO and $BiVO_4$ was confirmed after the fabrication of the ZnO/$BiVO_4$ photocatalyst via a facile ultrasonication method.

The textural properties of the samples were examined from a nitrogen (N_2) adsorption−desorption isotherm. According to the IUPAC classification, the samples showed a type IV isotherm, as seen in Figure 5a.[5] The ZnO/$BiVO_4$ catalyst showed a specific surface area of 4.2 m^2/g, which is greater than that of bare ZnO. In addition, a Barett−Joyner−Halenda pore volume of about 0.32 cm^3/g and an average pore diameter of about 310 nm were reported. The size distribution is shown in Figure 5b.

Figure 6a shows the UV−vis diffuse reflectance spectra of the samples. The band gap of each sample was determined by the Kubelka−Munk formula, as seen in Figure 6b.[5,16,17] Accordingly, the absorption edge values of 387 and 585 nm were detected from pristine ZnO and bare $BiVO_4$, respectively. After the creation of the binary composites, two absorption edge values at 397 and 585 nm were found. The former might be due to the contribution from the generated heterojunction, with a slight shift of the absorption edge, while the latter is mainly due to the contribution from the $BiVO_4$ photocatalyst. The corresponding band gap values of bare ZnO and pristine $BiVO_4$ were 3.20 and 2.12 eV, respectively. It should be noted that a slight shift of the band gap toward visible light was obtained after the creation of the ZnO/$BiVO_4$ heterojunction. This will result in an increase in the resultant photoactivity under natural sunlight.

To roughly compare the charge carrier separation efficiency in the prepared photocatalysts, the PL spectroscopic method was performed.[65] According to the PL spectra in Figure 6c,d, the ZnO/$BiVO_4$ photocatalyst provided the lowest intensity in the PL spectra, compared to pristine components, implying the lowest charge carrier recombination rate found in this sample. Therefore, the highest photocatalytic performance, compared to that of ZnO and $BiVO_4$, would be observed.

The electrochemical technique was performed to determine the spatial transfer and separation of electron−hole pairs using the linear sweep voltammetry (LSV) and electrochemical impedance spectroscopy (EIS) methods.[16,17] The highest current density was obtained from ZnO/$BiVO_4$, compared to the bare photocatalysts (Figure 7a), suggesting that the highest photoactivity could be found from this sample. The successful generation of the heterojunction photocatalyst provides an improvement of charge separation efficiency, causing an increase in the resultant photoactivity.[5,6,19] The result agrees well with the trend of relative intensity found in the PL spectra.

The charge recombination rate was estimated by performing EIS. In principle, the arc radius provides the information concerning the charge transfer process at the electrode/electrolyte interface. The lowest radius being obtained from the ZnO/$BiVO_4$ photocatalyst (Figure 7b) implies the lowest charge-transfer resistance, indicating that the greatest photocatalytic performance is expected to be detected from the ZnO/$BiVO_4$ heterojunction, compared to that of bare ZnO and pristine $BiVO_4$. It can be concluded that the results from the PL spectra, the LSV plots, and the EIS plots confirm the enhanced photoactivity of the prepared heterojunction, in comparison to those obtained from the individual photocatalysts.

To understand the mechanism regarding the enhanced efficiency of the photocatalyst, the Mott−Schottky plots were elucidated for the determination of the band structures of the heterojunction (Figure 7c). The details have been shown previously.[5,17] The flat band (V_{FB}) level of bare ZnO was found to be −0.16 eV, while that of pristine $BiVO_4$ was about 0.17 eV. The values are nearly the same as the conduction band (V_{CB}) levels of the photocatalysts[5,6] such that the V_{CB} values of ZnO and $BiVO_4$ were found to be −0.16 and 0.17 eV, respectively (see Figure 7c). The prepared ZnO (E_g of 3.20 eV) showed the V_{VB} level of 3.04 eV. $BiVO_4$ (E_g of 2.12 eV) displayed the V_{VB} value of 2.29 eV. In summary, the values of V_{CB} and V_{VB} levels obtained from both ZnO and $BiVO_4$ are depicted later in Figure 13. The charge transfer between ZnO and $BiVO_4$ was also proposed.

3.2. Photodegradation Study. The photocatalytic degradation of the RR141 dye and OTC antibiotic was investigated under both simulated UV light and natural solar light.

3.2.1. Photodegradation of the Pollutants under UV Light. Photodegradation of the OTC antibiotic and RR141 dye after UV light irradiation (a mercury lamp, 125 W) was studied. As seen in Figure 8a, lowering of OTC content with time indicates the removal of this antibiotic. The photolysis of OTC is negligible. Less than 5% removal of OTC via the adsorption process was detected in the presence of ZnO/

https://doi.org/10.1021/acsomega.2c07020
ACS Omega 2023, 8, 4835−4852

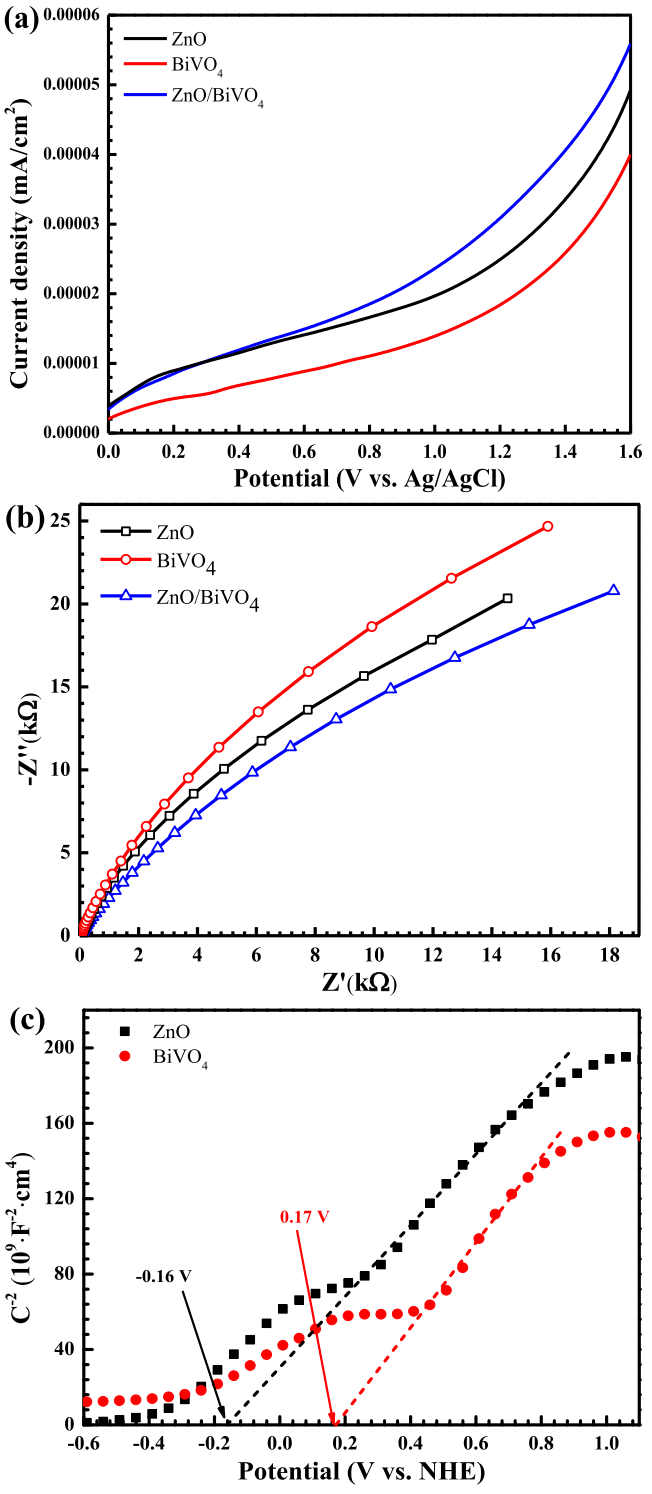

Figure 7. LSV scans plots (a), EIS Nyquist plots (b), and Mott–Schottky plots (c) of the samples using a frequency of 30 Hz in 0.1 M Na_2SO_4.

$BiVO_4$. Interestingly, enhanced detoxification of OTC was detected under light illumination. The photoactivity of about 88% was reported after 240 min (Figure 8c). The photoactivity of the binary heterojunction is about 1.5 and 1.9 times higher than those obtained from bare ZnO and pristine $BiVO_4$, respectively.

On examining the RR141 degradation, Figure 8b shows a decrease of RR141 concentration with time. The photolysis of the RR141 dye can be neglected. In addition, in the presence of ZnO/$BiVO_4$, lower than 13% of RR141 was removed via the adsorption process. Interestingly, enhanced photocatalytic degradation of RR141 under UV light was detected. The photoactivity reaches about 97% after 240 min (Figure 8d). For comparison, the physical mixture of ZnO and $BiVO_4$ was also used as a photocatalyst. However, this sample still shows lower performance than the ZnO/$BiVO_4$ photocatalyst. The result strongly indicates that the most important role is of the heterojunction photocatalyst for the improvement of the resultant photoactivity. As seen from Figure 8d, the heterojunction provides an enhanced performance, which is about 1.04, 2.66, and 1.03 times greater than those reported from bare ZnO, pristine $BiVO_4$, and the physical mixture, respectively, after 180 min.

The photodegradation reaction of both the OTC antibiotic and RR141 dye follows the first-order reaction (Figure 8e,f). The rate constants (k) of 0.0104 and 0.0157 min^{-1} were observed after UV light irradiation. ZnO/$BiVO_4$ shows the highest rate constants among all prepared samples. This correlates well with the greatest efficiency found in the heterojunction presented previously. On examining OTC removal (Figure 8e), ZnO/$BiVO_4$ shows a rate constant that is about 2.08 and 2.97 times greater than those of ZnO and $BiVO_4$, respectively. On examining RR141 degradation (Figure 8f), it is noted that the ZnO/$BiVO_4$ heterojunction provides a rate constant that is about 1.89, 4.76, and 1.43 times greater than those obtained from bare ZnO, pristine $BiVO_4$, and the physical mixture, respectively. All in all, the greatest photodegradation efficiency together with the highest rate constant found in the ZnO/$BiVO_4$ heterojunction photocatalyst is mainly due to the enhancement of the surface area, compared to that of bare ZnO, and the suppression of the charge carrier recombination rate after successful construction of the binary heterostructure.

3.2.2. Photodegradation of the Pollutants under Natural Sunlight. The photocatalytic degradation of OTC and RR141 was also studied under sunlight, as seen in Figure 9. By determining OTC degradation, an efficiency of about 95% was achieved after 80 min, in the presence of the ZnO/$BiVO_4$ photocatalyst (Figure 9a). Accordingly, a rate constant of about 0.0479 min^{-1} was obtained (Figure 9c). It can be clearly seen that the ZnO/$BiVO_4$ heterojunction shows the highest efficiency and the greatest rate constant in comparison to those of bare ZnO and pristine BVO_4. In the case of RR141 degradation, the same trend was also observed. With the addition of ZnO/$BiVO_4$, the highest performance reached 100% after only 80 of solar light irradiation (Figure 9b). The rate constant of 0.1071 min^{-1} was obtained. All in all, the results from both UV light and solar light support the enhanced photocatalytic performance of the binary heterojunction, compared to that of the individual photocatalysts. This is mainly due to the improvement of the surface area, compared to that of bare ZnO, and the remarkable enhancement of charge separation at the interface.

3.2.3. Influence of the Experimental Parameters on Photoactivity. The influence of some experimental parameters on OTC degradation was investigated. It can be seen from Figure 10a that increasing OTC concentration results in lowering of degradation efficiency. The enhancement of OTC concentration results in much more absorption of light by the OTC molecules instead of the catalyst. Therefore, a decrease of photon flux reaching the photocatalyst causes the lowering

https://doi.org/10.1021/acsomega.2c07020
ACS Omega 2023, 8, 4835−4852

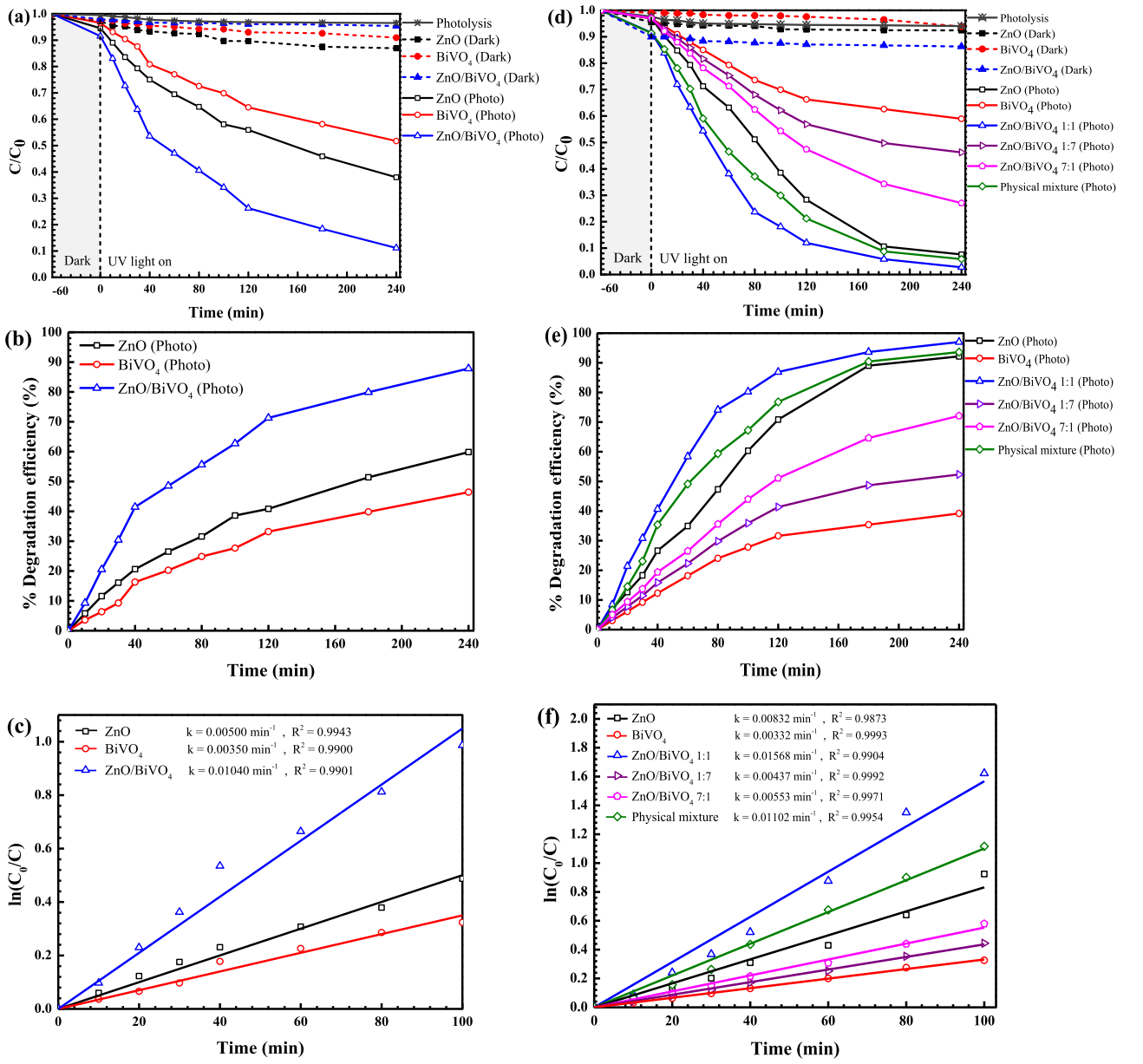

Figure 8. Plots of OTC antibiotic concentration (a) and RR141 dye (b) vs time, the photodegradation efficiency of OTC (c) and RR141 (d) degradation, and $\ln(C_0/C)$ vs time obtained from the photodegradation of the OTC antibiotic (e) and RR141 (f).

of the resultant photocatalytic performance. The addition of 20 ppm OTC showed the lowest photoactivity. It should be noted that after 240 min, the efficiency reached about 90% with an initial OTC concentration of 10 ppm. Thus, this concentration was used for further study.

The effect of photocatalyst content on photocatalytic performance was also elucidated. As seen in Figure 10b, the addition of a catalyst content of up to 50 mg causes an increase in photoactivity, resulting from the enhancement of OTC adsorption on the photocatalyst surface together with the increment of the photocatalyst density over one unit area of photo irradiation.[5,17] However, a drop of the performance was found after 75 mg of the catalyst was added. Therefore, the catalyst loading was fixed at 50 mg for further investigation.

The effect of the initial solution pH (3−11) on photocatalytic activity was also elucidated (Figure 10c). The OTC aqueous solution showed the natural solution pH of 7. A drastic decrease of the photocatalytic performance at an extremely acidic condition (pH = 3) is mainly assigned to the dissolution of the photocatalyst. On examining the extreme basic condition of pH = 11, in principle, a negative charge on the photocatalyst surface and a negative charge of OTC molecules (pK_a = 3.57, 7.79, and 9.88) co-existed.[5,17] This causes the repulsion between the photocatalyst and the OTC antibiotic so that the lowering of the performance could be expected. However, the pH of about 11 provides the highest photoactivity compared to the natural pH of about 7. This can be explained in terms of the much higher production of active species such as hydroxyl radicals under the basic condition.[16,17] The higher the number of active radicals, the greater the resultant photoactivity.

Furthermore, the influence of some parameters on RR141 degradation was also elucidated (see Figure 11). First, the lowest dye concentration of 5 ppm showed the greatest performance (Figure 11a). A decrease of the efficiency with an increment of dye concentration was observed. However, 10

https://doi.org/10.1021/acsomega.2c07020
ACS Omega 2023, 8, 4835−4852

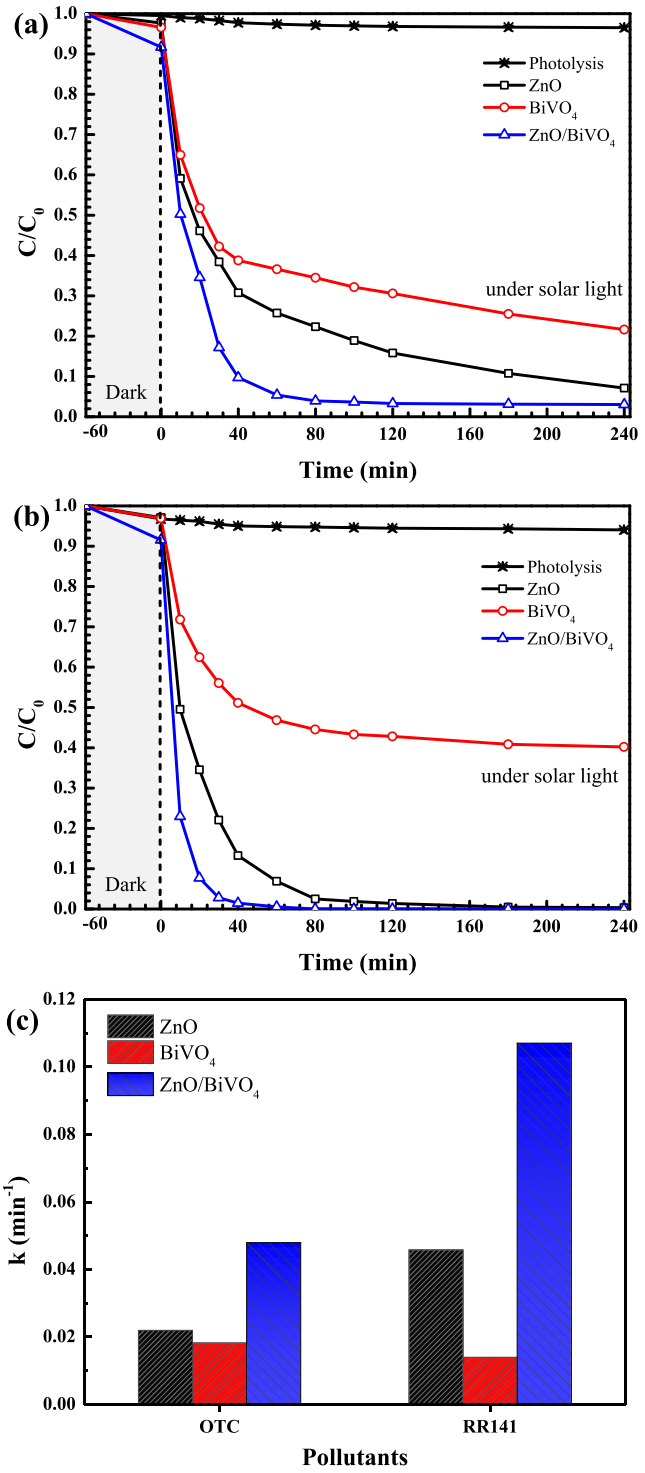

Figure 9. Lowering of OTC antibiotic (a) and RR141 dye (b) concentrations with time under natural sunlight and the rate constants of the photocatalysts toward the degradation of the OTC antibiotic and RR141 dye (c).

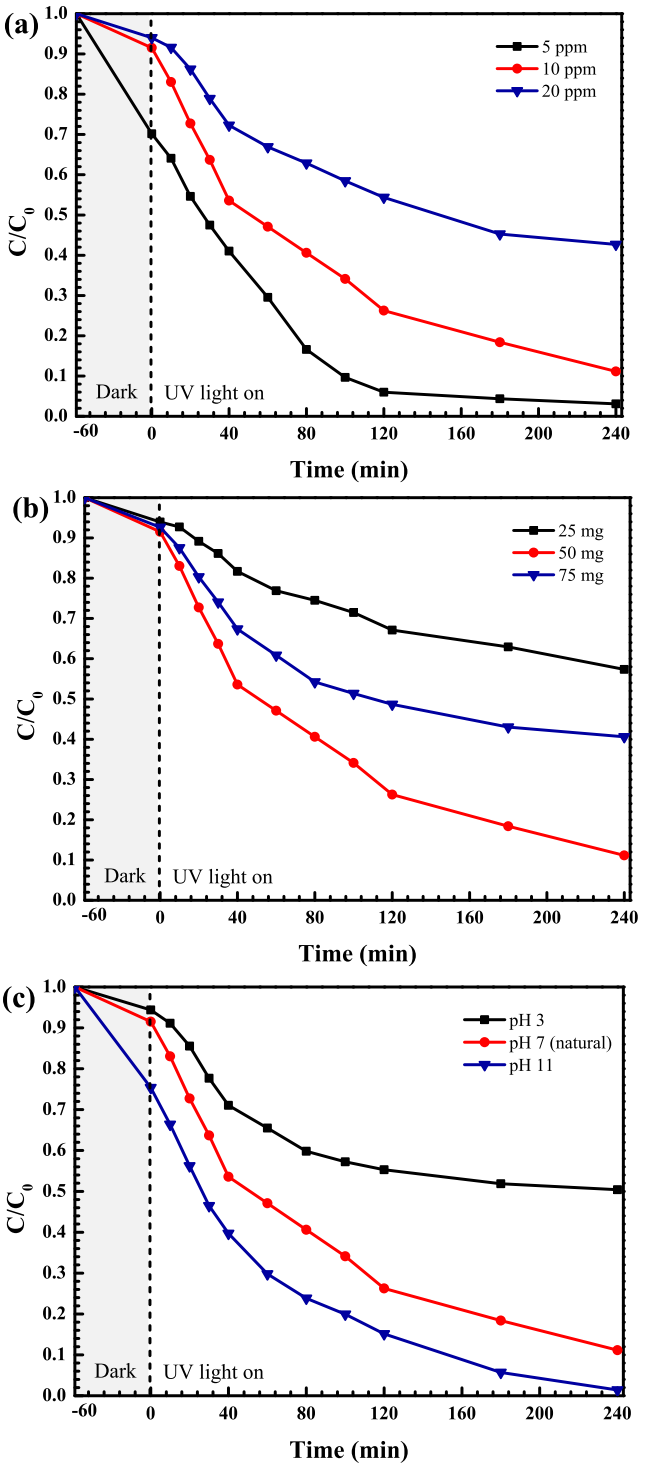

Figure 10. Effect of initial concentration (a), catalyst content (b), and initial solution pH (c) on photodegradation of the OTC antibiotic.

ppm of RR141 is the optimal concentration for further investigation. Second, the effect of the catalyst content on the efficiency is shown in Figure 11b. An increase in the catalyst loading of up to 50 mg provided the maximum photoactivity within 240 min. Third, the influence of pH on the photocatalytic activity was studied over the pH range of 3−11 (Figure 11c). The natural pH of the dye solution is about 7. A dramatic drop of the performance at a pH of 3 was mainly due to the dissolution of the prepared photocatalyst under the acidic condition. The performance obtained from the natural pH of 7 showed the efficiency to be as high as that obtained from the basic condition (pH of 11). Therefore, the result confirms no need to adjust the initial solution pH of the RR141 dye.

3.2.4. Photodegradation Mechanism and Recycling Ability. The photodegradation mechanism of the OTC

https://doi.org/10.1021/acsomega.2c07020
ACS Omega 2023, 8, 4835−4852

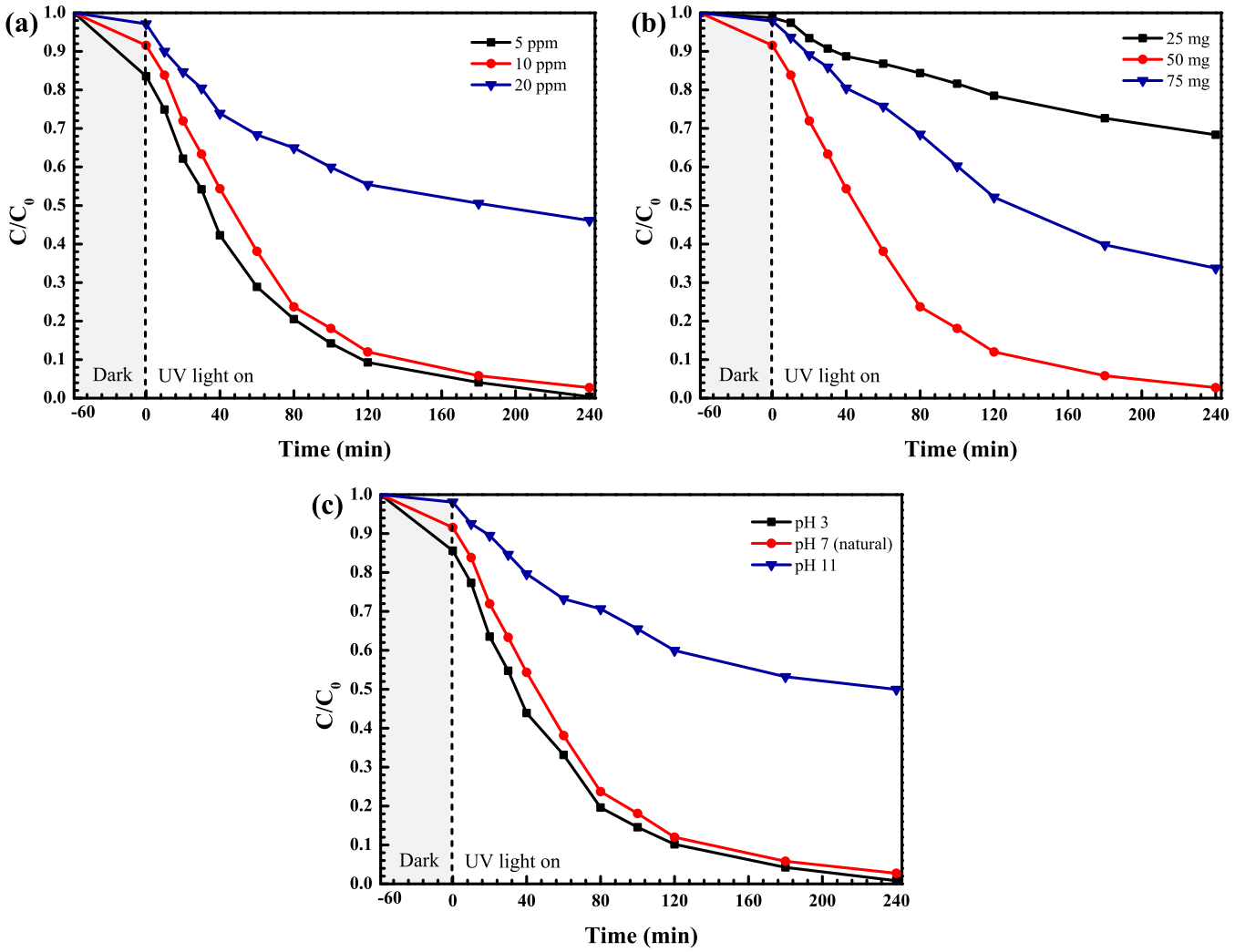

Figure 11. Effect of initial concentration (a), catalyst content (b), and initial solution pH (c) on photodegradation of the RR141 dye.

antibiotic was examined by the trapping method.[5,16,17] The photoactivity, in the presence of various quenchers, was elucidated. A dramatic decrease of photoactivity was observe after the addition of IPA (Figure 12a,b), implying the most important role of the hydroxyl radicals in the degradation of the antibiotic. The rate constant also decreases with the addition of IPA (Figure 12c). In addition, photogenerated holes play a subordinate role in the removal of the pollutants.

Furthermore, monitoring of the hydroxyl radical ($^{\bullet}OH$) after light irradiation was carried out via the TA probe technique.[17] The fluorescence product, 2-hydroxyterephthalic acid (TA-OH), was detected. The increasing of PL peak intensity at 425 nm with increasing irradiation time was clearly observed, as seen in Figure 12d. Again, the result strongly confirms the major role of the hydroxyl radicals in the degradation of the toxic pollutant.

Upon light irradiation, the photogeneration of the electrons and holes were occurred in the conduction band (CB) and the valence band (VB), respectively. After that, the formation of reactive species would be expected. In principle, the energy level of the CB and VB edges of both $BiVO_4$ and ZnO photocatalysts can be determined by using the Mulliken electronegativity theory as follows

$$E_{VB} = \chi - E_C + 0.5E_g \quad (4)$$

$$E_{CB} = E_{VB} - E_g \quad (5)$$

where E_{VB} is the VB potential, E_{CB} is the CB potential, E_C is the standard hydrogen electrode potential (≈4.5 eV), and χ is the absolute value of the electronegativity of the semiconducting photocatalyst.[3,6,16] The values of the electronegativity were 2.34 and 5.79 eV, respectively, for $BiVO_4$ and ZnO.[3,6,16] In theory, the VB and CB potentials of the $BiVO_4$ photocatalyst were found to be 2.71 and 0.37 eV, respectively, while the corresponding values of the ZnO photocatalyst were found to be 2.90 and −0.31 eV, respectively. In practice, however, after the creation of the heterojunction, the CB potential levels of ZnO and $BiVO_4$ are found to be −0.16 and 0.17 eV, respectively, as shown previously from the Mott−Schottky plots in Figure 7c. The band gap energy of ZnO and $BiVO_4$ are 3.20 and 2.12 eV, respectively. Therefore, the VB potential levels of 3.04 and 2.29 eV can be obtained for ZnO and $BiVO_4$, respectively.

To determine the heterojunction photocatalyst, the creation of a heterostructure based on the coupling of two photocatalysts has been demonstrated.[39,47,69−71] The type II and Z-scheme heterojunctions were previously proposed. However, it is accepted that the electron transfer mechanism of the traditional Z-scheme photocatalyst and all-solid-state Z-scheme photocatalyst still exhibit some drawbacks. Alternatively, the

https://doi.org/10.1021/acsomega.2c07020
ACS Omega 2023, 8, 4835−4852

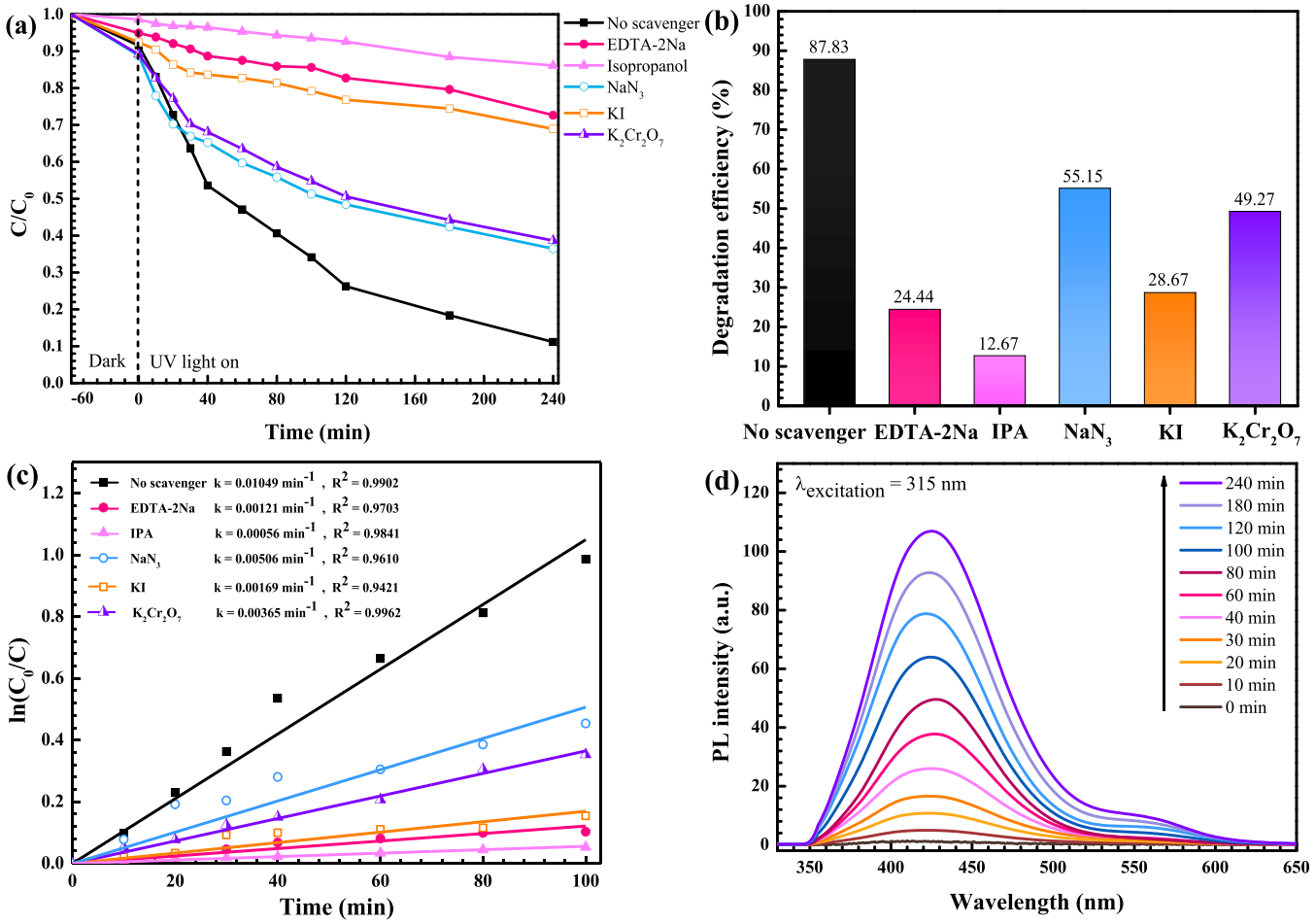

Figure 12. Lowering of C/C_0 due to photodegradation (a), bar chart showing photodegradation efficiency (b), rate constants of the photocatalysts toward degradation of the OTC antibiotic after the addition of various scavengers (c), and hydroxyl radical trapping PL spectra of the solution after photo-illumination of the $ZnO/BiVO_4$ photocatalyst (d).

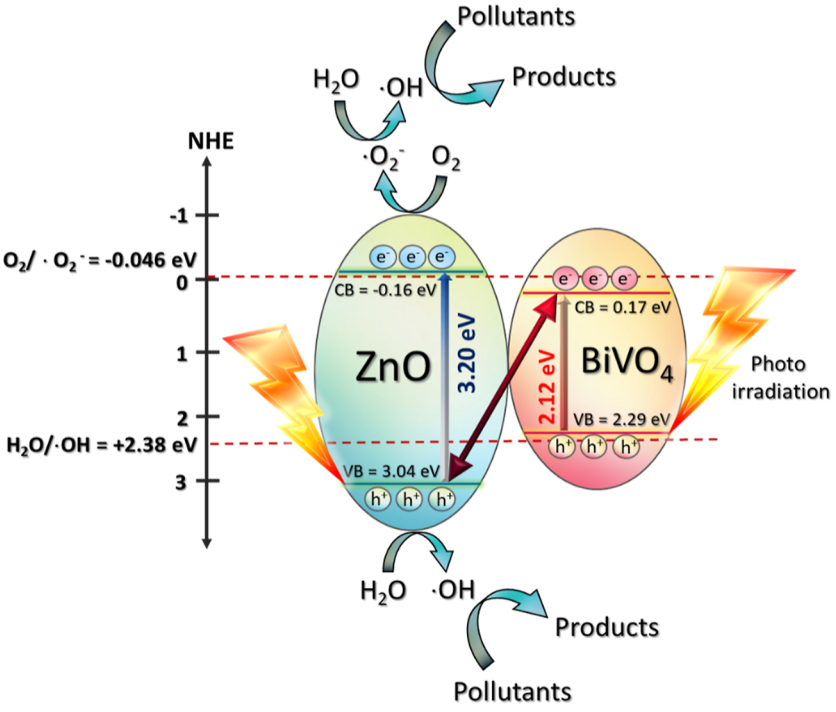

Figure 13. Photocatalytic mechanism schemes based on degradation of the pollutants after photoirradiation of the $ZnO/BiVO_4$ photocatalyst.

https://doi.org/10.1021/acsomega.2c07020
ACS Omega 2023, 8, 4835−4852

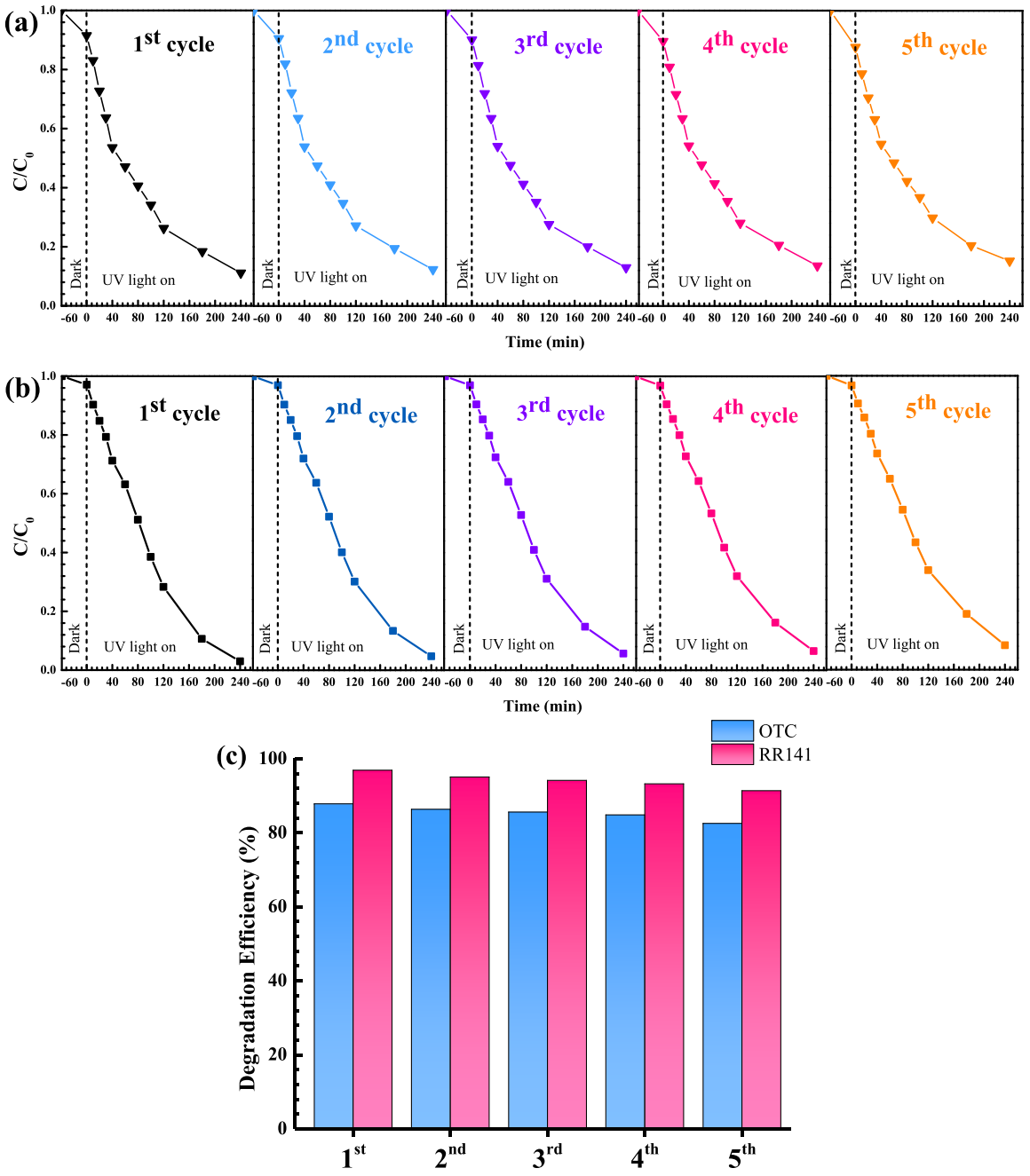

Figure 14. Reusability of the $ZnO/BiVO_4$ photocatalyst for photodegradation of the OTC antibiotic (a) and RR141 dye (b) and the bar charts (c) showing the cycling ability of the photocatalyst.

novel model based on a S-scheme photocatalyst was proposed.[65−68] In this case, the charge separation and high redox ability are obtained. In theory, extended photoabsorption, excellent charge separation, and a strong redox potential are collectively gained. This heterojunction mechanism can be applied nicely in the present research. Therefore, the removal of toxic pollutants by the $ZnO/BiVO_4$ S-scheme heterojunction photocatalyst is proposed in Figure 13. The photocatalytic degradation of the toxic contaminant can be summarized as follows.

$$ZnO/BiVO_4 + h\nu \rightarrow ZnO/BiVO_4 + e^- + h^+ \quad (6)$$

$$e^- + O_2 \rightarrow {}^{\bullet}O_2^- \quad (7)$$

$${}^{\bullet}O_2^- + 2H_2O + e^- \rightarrow 2{}^{\bullet}OH + 2OH^- \quad (8)$$

$$h^+ + OH^- \rightarrow {}^{\bullet}OH \quad (9)$$

$${}^{\bullet}OH + \text{contaminant} \rightarrow \text{products} \quad (10)$$

$$h^+ + \text{contaminant} \rightarrow \text{products} \quad (11)$$

Reusability is a crucial factor influencing the practical use of the synthesized photocatalyst.[5,6,16,17] Thus, the cycling ability of the photocatalyst after the removal of the RR141 dye and OTC antibiotic was studied. The $ZnO/BiVO_4$ photocatalyst still provides high photocatalytic performance even after five cycles of use (Figure 14). The chemical structural of the photocatalyst after pollutant degradation was investigated. The

https://doi.org/10.1021/acsomega.2c07020
ACS Omega 2023, 8, 4835−4852

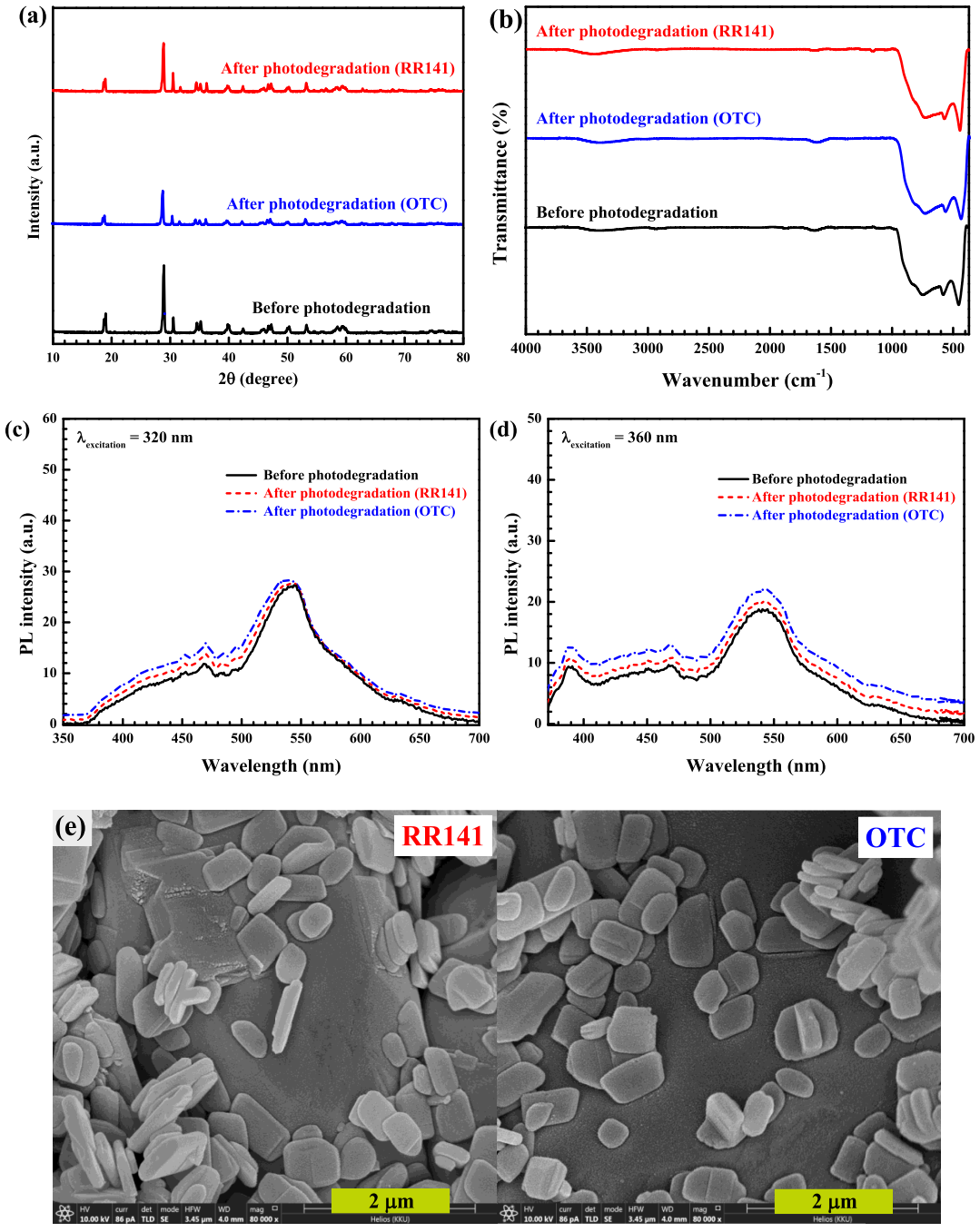

Figure 15. XRD patterns (a), vibrational spectra (b), and PL spectra using $\lambda_{excitation}$ values of 320 (c) and 360 nm (d) of the fresh and used photocatalyst and SEM images of the ZnO/$BiVO_4$ photocatalyst after the removal of the RR141 dye and OTC antibiotic (e).

stability of the structure was confirmed (Figure 15a). The identical FT-IR spectra (Figure 15b) and PL spectra (Figure 15c,d) suggested the chemical stability of the photocatalyst as well. Additionally, the morphology of the used photocatalyst (Figure 15e) is more or less the same as that received from the fresh photocatalyst (Figure 2), implying the stability of the sample morphology.

It is important to noted that leaching of Zn^{2+} after photodegradation was also one major concern. The measurement of Zn^{2+} in the solution was performed. It can be shown that bare ZnO showed 7 ppm Zn^{2+} in the pollutant solution, while ZnO/$BiVO_4$ exhibited only 0.7 ppm Zn^{2+}. The result strongly confirms the improvement of the photocatalyst stability after the creation of the heterojunction. The photoactivity of various catalysts toward degradation of the RR141 dye and OTC antibiotic has been studied.[1,6,7,13,16,17,20,21,72−84] In this work, the ZnO/$BiVO_4$ photocatalyst is used for the degradation of the toxic pollutants under UV light and natural sunlight. The performance of the synthesized photocatalyst together with those reported in the literature is shown in Table 1. By determining RR141 degradation, bare ZnO provided the photoactivity of 95−98%.[6,72,76] Capped ZnO, by using sodium dodecyl sulfate (SDS) or polyvinylpyrrolidone (PVP), showed the performance of 60−100%.[1,7,73] In the case of metal-doped ZnO, copper-doped ZnO and lead-doped ZnO displayed the

https://doi.org/10.1021/acsomega.2c07020
ACS Omega 2023, 8, 4835−4852

Table 1. Comparison of the RR141 Azo Dye and OTC Antibiotic Degradation by Using Various Photocatalysts

catalyst	concentration (mg L^{-1})	catalyst loading (mg)	light source	lamp (W)	time (min)	photodegradation (%)	refs
Photodegradation of RR141 Azo Dye							
ZnO	10	50	UV	125	240	95	72
ZnO	10	50	UV	125	240	98	6
ZnO	30	30	UV		120	96	76
SDS-capped ZnO	10	50	UV	125	240	100	1
SDS-capped ZnO	10	50	UV	125	240	95	7
SDS-capped ZnO	10	50	visible	15	240	60	7
SDS-capped ZnO	10	50	solar light		240	88	7
PVP-capped ZnO	10	50	UV	125	120	100	73
Cu−ZnO	50	100	UV		120	89	77
3% Pb−ZnO	30	30	UV		120	96	76
ZnO/CdS	10	50	visible	15	120	80	6
Bi_2MoO_6	10	50	UV	125	240	37	74
Bi_2MoO_6	10	50	visible	15	240	45	74
Bi_4MoO_9	10	50	UV	125	240	68	75
Bi_4MoO_9	10	50	solar light		240	70	75
ZnO−$BiVO_4$	10	50	UV	125	240	97	this work
ZnO−$BiVO_4$	10	50	solar light		60	100	this work
Photodegradation of OTC Antibiotic							
ZnO	10	100	visible	300	150	50	78
$BiVO_4$	10	50	visible	15	240	55.5	17
$BiVO_4$	10	50	natural sunlight		240	82.8	17
$BiVO_4$	10	50	visible	15	240	62	16
$BiVO_4$	10	50	solar light		240	93	16
$BiVO_4$	10	50	visible	1000	120	61.1	13
$BiVO_4$	10	20	visible	300	120	52.7	79
$BiVO_4/TiO_2$	10		visible	1000	120	68.4	20
$Bi_2S_3/BiVO_4$	200	100	visible	500	960	67	80
ZnO−TiO_2	60	5	solar light		8	90.3	81
Cu doped ZnO-MWCNT	50	5	visible	400	240	55	82
NiCo/ZnO/g-C_3N_4	10	20	visible	300	50	71.3	83
Ag/AgCl/$BiVO_4$	20	50	UV	1000	120	97.6	13
Ag/Ag_2S/$BiVO_4$	20	20	visible	500	150	99.8	21
Ag/$BiVO_4$/GO	20	100	visible	500	70	90	84
ZnO/$ZnFe_2O_4$/diatomite	10	100	visible	300	150	95	78
ZnO−$BiVO_4$	10	50	UV	125	240	88	this work
ZnO−$BiVO_4$	10	50	solar light		100	95	this work

performances of 89 and 96%, respectively.[76,77] The ZnO/CdS composite exhibited the photoactivity of 80%.[6] In addition, the pristine bismuth molybdate photocatalyst showed the efficiency of 37−70%.[74,75] Interestingly, in the present work, the ZnO/$BiVO_4$ heterojunction showed the performances of 97 and 100% under UV light and sunlight, respectively. In terms of OTC removal, bare ZnO showed the efficiency of 50% after 150 min of visible light irradiation.[78] In the case of pristine $BiVO_4$, the performance of 52−93% was detected.[13,16,17,79] The binary composites based on $BiVO_4$ showed a high efficiency of about 68% .[20,80] The ZnO−TiO_2 photocatalyst provided the performance of 90%.[81] Enhancement of the efficiency to about 55−99.8% was reported in the ternary composites based on either ZnO or $BiVO_4$.[13,21,74,82−84] In the present work, the prepared ZnO/$BiVO_4$ catalyst exhibited high photocatalytic performances of 88 and 95% under UV light and sunlight, respectively. To sum up, the prepared heterojunction catalyst displayed enhanced performance toward the degradation of the RR141 dye and OTC antibiotic under the economical natural sunlight. The synthesis of the photocatalyst can be performed perfectly without the doping of expensive noble metals such as gold or silver. The present research shows the novel route for detoxification of the harmful dye and antibiotic in aqueous solution by utilization of the abundant solar energy.

4. CONCLUSIONS

The ZnO/$BiVO_4$ S-scheme photocatalyst has been generated very easily by a facile hydrothermal technique followed by an ultrasonic route. The prepared ZnO/$BiVO_4$ heterojunction showed the improvement of the surface area, compared to that of bare ZnO. The heterojunction also exhibited the lowest PL intensity, compared to those of bare ZnO and $BiVO_4$. Accordingly, the heterostructure photocatalyst showed the enhanced sunlight-active photocatalytic activities of 100 and 95% toward degradation of the RR141 dye and OTC antibiotic, respectively. The photodegradation of the pollutant follows the first-order kinetic model. Hydroxyl radicals play the most important role in the removal of the toxic pollutants. The synthesized ZnO/$BiVO_4$ photocatalyst still maintains excellent performance even after five cycles of use, indicating its promising cycling ability. The present finding demonstrates a promising avenue to fabricate a novel sunlight active S-scheme heterostructure photocatalyst for environmental remediation.

https://doi.org/10.1021/acsomega.2c07020
ACS Omega 2023, 8, 4835−4852

AUTHOR INFORMATION

Corresponding Author

Suwat Nanan − *Materials Chemistry Research Center, Department of Chemistry and Center of Excellence for Innovation in Chemistry (PERCH-CIC), Faculty of Science, Khon Kaen University, Khon Kaen 40002, Thailand;* orcid.org/0000-0002-8737-689X; Phone: +66 43 202222 41 ext. 12370; Email: suwatna@kku.ac.th; Fax: +66 43 202373

Authors

Khemika Wannakan − *Materials Chemistry Research Center, Department of Chemistry and Center of Excellence for Innovation in Chemistry (PERCH-CIC), Faculty of Science, Khon Kaen University, Khon Kaen 40002, Thailand*

Kamonpan Khansamrit − *Materials Chemistry Research Center, Department of Chemistry and Center of Excellence for Innovation in Chemistry (PERCH-CIC), Faculty of Science, Khon Kaen University, Khon Kaen 40002, Thailand*

Teeradech Senasu − *Materials Chemistry Research Center, Department of Chemistry and Center of Excellence for Innovation in Chemistry (PERCH-CIC), Faculty of Science, Khon Kaen University, Khon Kaen 40002, Thailand*

Complete contact information is available at: https://pubs.acs.org/10.1021/acsomega.2c07020

Notes

The authors declare no competing financial interest.

ACKNOWLEDGMENTS

We would like to thank the fund from Materials Chemistry Research Center (MCRC), Khon Kaen University, Thailand. S.N. would like to thank the fund supported by Research and Graduate Studies, Khon Kaen University (Research Program, grant number RP64-2-Canabis/001), fiscal year 2021. S.N. also wishes to acknowledge the financial support from the Center of Excellence for Innovation in Chemistry (PERCH-CIC) and the Center of Excellence in Petrochemical and Materials technology (PETROMAT), Ministry of Higher Education, Science, Research, and Innovation.

REFERENCES

(1) Juabrum, S.; Chankhanittha, T.; Nanan, S. Hydrothermally Grown SDS-Capped ZnO Photocatalyst for Degradation of RR141 Azo Dye. *Mater. Lett.* **2019**, *245*, 1−5.

(2) Mokhtari-Shourijeh, Z.; Langari, S.; Montazerghaem, L.; Mahmoodi, N. M. Synthesis of Porous Aminated PAN/PVDF Composite Nanofibers by Electrospinning: Characterization and Direct Red 23 Removal. *J. Environ. Chem. Eng.* **2020**, *8*, 103876.

(3) Chankhanittha, T.; Yenjai, C.; Nanan, S. Utilization of Formononetin and Pinocembrin from Stem Extract of Dalbergia Parviflora as Capping Agents for Preparation of ZnO Photocatalysts for Degradation of RR141 Azo Dye and Ofloxacin Antibiotic. *Catal. Today* **2022**, *384-386*, 279−293.

(4) Mahmoodi, N. M.; Keshavarzi, S.; Oveisi, M.; Rahimi, S.; Hayati, B. Metal-Organic Framework (ZIF-8)/Inorganic Nanofiber (Fe_2O_3) Nanocomposite: Green Synthesis and Photocatalytic Degradation Using LED Irradiation. *J. Mol. Liq.* **2019**, *291*, 111333.

(5) Chankhanittha, T.; Komchoo, N.; Senasu, T.; Piriyanon, J.; Youngme, S.; Hemavibool, K.; Nanan, S. Silver Decorated ZnO Photocatalyst for Effective Removal of Reactive Red Azo Dye and Ofloxacin Antibiotic under Solar Light Irradiation. *Colloids Surf., A* **2021**, *626*, 127034.

(6) Senasu, T.; Chankhanittha, T.; Hemavibool, K.; Nanan, S. Visible-Light-Responsive Photocatalyst Based on ZnO/CdS Nanocomposite for Photodegradation of Reactive Red Azo Dye and Ofloxacin Antibiotic. *Mater. Sci. Semicond. Process.* **2021**, *123*, 105558.

(7) Kakarndee, S.; Nanan, S. SDS Capped and PVA Capped ZnO Nanostructures with High Photocatalytic Performance toward Photodegradation of Reactive Red (RR141) Azo Dye. *J. Environ. Chem. Eng.* **2018**, *6*, 74−94.

(8) Kumar, A.; Subash, B.; Krishnakumar, B.; Sobral, A. J. F. N.; Sankaran, K. R. Synthesis Characterization and Excellent Catalytic Activity of Modified ZnO Photocatalyst for RR 120 Dye Degradation under UV-A and Solar Light Illumination. *J. Water Proc. Eng.* **2016**, *13*, 6−15.

(9) Kalaiarasan, S.; Uthirakumar, P.; Shin, D.; Lee, I. H. The Degradation Profile of High Molecular Weight Textile Reactive Dyes: A Daylight Induced Photocatalytic Activity of ZnO/Carbon Quantum Dot Photocatalyst. *Environ. Nanotechnol., Monit. Manage.* **2021**, *15*, 100423.

(10) Almasian, A.; Mahmoodi, N. M.; Olya, M. E. Tectomer Grafted Nanofiber: Synthesis, Characterization and Dye Removal Ability from Multicomponent System. *J. Ind. Eng. Chem.* **2015**, *32*, 85−98.

(11) Mahmoodi, N. M.; Karimi, B.; Mazarji, M.; Moghtaderi, H. Cadmium Selenide Quantum Dot-Zinc Oxide Composite: Synthesis, Characterization, Dye Removal Ability with UV Irradiation, and Antibacterial Activity as a Safe and High-Performance Photocatalyst. *J. Photochem. Photobiol., B* **2018**, *188*, 19−27.

(12) Ye, S.; Zhou, X.; Xu, Y.; Lai, W.; Yan, K.; Huang, L.; Ling, J.; Zheng, L. Photocatalytic Performance of Multi-Walled Carbon Nanotube/$BiVO_4$ Synthesized by Electro-Spinning Process and Its Degradation Mechanisms on Oxytetracycline. *J. Chem. Eng.* **2019**, *373*, 880−890.

(13) Dai, Y.; Liu, Y.; Kong, J.; Yuan, J.; Sun, C.; Xian, Q.; Yang, S.; He, H. High Photocatalytic Degradation Efficiency of Oxytetracycline Hydrochloride over Ag/AgCl/$BiVO_4$ Plasmonic Photocatalyst. *Solid State Sci.* **2019**, *96*, 105946.

(14) Jia, L.; Jin, Y.; Li, J.; Wei, Z.; Chen, M.; Ma, J. Study on High-Efficiency Photocatalytic Degradation of Oxytetracycline Based on a Spiral Microchannel Reactor. *Ind. Eng. Chem. Res.* **2022**, *61*, 554−565.

(15) Xu, J.; Bian, Z.; Xin, X.; Chen, A.; Wang, H. Size Dependence of Nanosheet BiVO4 with Oxygen Vacancies and Exposed {0 0 1} Facets on the Photodegradation of Oxytetracycline. *J. Chem. Eng.* **2018**, *337*, 684−696.

(16) Hemavibool, K.; Sansenya, T.; Nanan, S. Enhanced Photocatalytic Degradation of Tetracycline and Oxytetracycline Antibiotics by $BiVO_4$ Photocatalyst under Visible Light and Solar Light Irradiation. *J. Antibiot.* **2022**, *11*, 761.

(17) Senasu, T.; Youngme, S.; Hemavibool, K.; Nanan, S. Sunlight-Driven Photodegradation of Oxytetracycline Antibiotic by $BiVO_4$ Photocatalyst. *J. Solid State Chem.* **2021**, *297*, 122088.

(18) Xu, W.; Zhang, Q.; Xu, K.; Qiu, L.; Song, J.; Wang, L. Study on Visible Light Photocatalytic Performance of $BiVO_4$ Modified by Graphene Analogue Boron Nitride. *Chemosphere* **2022**, *307*, 135811.

(19) Lakhera, S. K.; Hafeez, H. Y.; Venkataramana, R.; Veluswamy, P.; Choi, H.; Neppolian, B. Design of a Highly Efficient Ternary AgI/RGO/$BiVO_4$ Nanocomposite and Its Direct Solar Light Induced Photocatalytic Activity. *Appl. Surf. Sci.* **2019**, *487*, 1289−1300.

(20) Wang, W.; Han, Q.; Zhu, Z.; Zhang, L.; Zhong, S.; Liu, B. Enhanced Photocatalytic Degradation Performance of Organic Contaminants by Heterojunction Photocatalyst $BiVO_4$/TiO_2/RGO and Its Compatibility on Four Different Tetracycline Antibiotics. *Adv. Powder Technol.* **2019**, *30*, 1882−1896.

(21) Wei, Z.; Benlin, D.; Fengxia, Z.; Xinyue, T.; Jiming, X.; Lili, Z.; Shiyin, L.; Leung, D. Y. C.; Sun, C. A Novel 3D Plasmonic P-n Heterojunction Photocatalyst: Ag Nanoparticles on Flower-like p-Ag_2S/n-$BiVO_4$ and Its Excellent Photocatalytic Reduction and Oxidation Activities. *Appl. Catal., B* **2018**, *229*, 171−180.

(22) Ali, A. A.; El Fadaly, E. A.; Deraz, N. M. Auto-Combustion Fabrication, Structural, Morphological and Photocatalytic Activity of

CuO/ZnO/MgO Nanocomposites. *Mater. Chem. Phys.* **2021**, *270*, 124762.
(23) Chuenpratoom, T.; Hemavibool, K.; Rermthong, K.; Nanan, S. Removal of Lead by Merlinoite Prepared from Sugarcane Bagasse Ash and Kaolin: Synthesis, Isotherm, Kinetic, and Thermodynamic Studies. *Molecules* **2021**, *26*, 7550.
(24) Wang, H.; Li, Z.; Yahyaoui, S.; Hanafy, H.; Seliem, M. K.; Bonilla-Petriciolet, A.; Luiz Dotto, G.; Sellaoui, L.; Li, Q. Effective Adsorption of Dyes on an Activated Carbon Prepared from Carboxymethyl Cellulose: Experiments, Characterization and Advanced Modelling. *J. Chem. Eng.* **2021**, *417*, 128116.
(25) Du, X.; Yang, W.; Liu, Y.; Zhang, W.; Wang, Z.; Nie, J.; Li, G.; Liang, H. Removal of Manganese, Ferrous and Antibiotics from Groundwater Simultaneously Using Peroxymonosulfate-Assisted in-Situ Oxidation/Coagulation Integrated with Ceramic Membrane Process. *Sep. Purif. Technol.* **2020**, *252*, 117492.
(26) Rajput, R. B.; Shaikh, R.; Sawant, J.; Kale, R. B. Recent Developments in ZnO-Based Heterostructures as Photoelectrocatalysts for Wastewater Treatment: A Review. *Environ. Adv.* **2022**, *9*, 100264.
(27) Jiang, C. H.; Yao, C. B.; Wang, Z. M.; Wang, X.; Wang, L. Y. Heterostructure MoS_2@ZnO Nanowires: Preparation, Ultrafast Nonlinear Optical Behavior and Photoelectric Functional Application. *Appl. Surf. Sci.* **2022**, *599*, 153920.
(28) Wang, J.; Feng, J.; Wei, C. Molecularly Imprinted Polyaniline Immobilized on Fe_3O_4/ZnO Composite for Selective Degradation of Amoxycillin under Visible Light Irradiation. *Appl. Surf. Sci.* **2023**, *609*, 155324.
(29) Choudhary, S.; Sharma, M.; Krishnan, V.; Mohapatra, S. Facile Synthesis, Structural, Morphological, Photocatalytic and Optical Properties of $CoFe_2O_4$/ZnO Hybrid Nanostructures. *Ceram. Int.* **2022**, *48*, 34033−34045.
(30) Ouriques Brasileiro, I. L.; Madeira, V. S.; Lopes-Moriyama, A. L.; Rodrigues de Almeida Ramalho, M. L. Addition of G-C_3N_4 to ZnO and $ZnFe_2O_4$ to Improve Photocatalytic Degradation of Emerging Organic Pollutants. *Ceram. Int.* **2023**, *49*, 4449−4459.
(31) Li, D.; Zhang, W.; Niu, Z.; Zhang, Y. Improvement of Photocatalytic Activity of BiOBr and BiOBr/ZnO under Visible-Light Irradiation by Short-Time Low Temperature Plasma Treatment. *J. Alloys Compd.* **2022**, *924*, 166608.
(32) Yang, X.; Sun, S.; Ye, L.; Yun, D.; Liu, C.; Guo, Y.; Yang, B.; Yang, M.; Yang, Q.; Liang, S.; Cui, J. One-Pot Integration of S-Doped BiOCl and ZnO into Type-II Photocatalysts: Simultaneously Boosting Bulk and Surface Charge Separation for Enhanced Antibiotic Removal. *Sep. Purif. Technol.* **2022**, *299*, 121725.
(33) uz Zaman, F.; Nagamuthu, S.; Cui, K.; Hou, L.; Yuan, C. Microwave-Assisted Synthesis of Porous Heterojunction ZnO/$ZnMn_2O_4$ Microrods for Efficient Degradation of Organic Pollutants. *Inorg. Chem. Commun.* **2022**, *144*, 109845.
(34) Ramesh Reddy, N. R.; Mohan Reddy, P. M.; Hak Jung, J. H.; Woo Joo, S. W. Construction of Various Morphological ZnO-NiO S-Scheme Nanocomposites for Photocatalytic Dye Degradation. *Inorg. Chem. Commun.* **2022**, *146*, 110107.
(35) Chen, Z.; Dedova, T.; Spalatu, N.; Maticiuc, N.; Rusu, M.; Katerski, A.; Acik, I. O.; Unold, T.; Krunks, M. ZnO/NiO Heterostructures with Enhanced Photocatalytic Activity Obtained by Ultrasonic Spraying of a NiO Shell onto ZnO Nanorods. *Colloids Surf., A* **2022**, *648*, 129366.
(36) Yang, J. S.; Wu, J. J. Low-Potential Driven Fully-Depleted $BiVO_4$/ZnO Heterojunction Nanodendrite Array Photoanodes for Photoelectrochemical Water Splitting. *Nano Energy* **2017**, *32*, 232−240.
(37) Srinivasan, N.; Anbuchezhiyan, M.; Harish, S.; Ponnusamy, S. Hydrothermal Synthesis of C Doped ZnO Nanoparticles Coupled with $BiVO_4$ and Their Photocatalytic Performance under the Visible Light Irradiation. *Appl. Surf. Sci.* **2019**, *494*, 771−782.
(38) Singh, S.; Sharma, R.; Mehta, B. R. Enhanced Surface Area, High Zn Interstitial Defects and Band Gap Reduction in N-Doped ZnO Nanosheets Coupled with $BiVO_4$ Leads to Improved Photocatalytic Performance. *Appl. Surf. Sci.* **2017**, *411*, 321−330.
(39) Raja, A.; Rajasekaran, P.; Vishnu, B.; Selvakumar, K.; Yeon Do, J.; Swaminathan, M.; Kang, M. Fabrication of Effective Visible-Light-Driven Ternary Z-Scheme ZnO-Ag-$BiVO_4$ Heterostructured Photocatalyst for Hexavalent Chromium Reduction. *Sep. Purif. Technol.* **2020**, *252*, 117446.
(40) Zhang, J.; Xie, L. Synthesis and Sonophotocatalytic Activities of ZnO\$BiVO_4$\$Co_3O_4$ Composites. *Chem. Phys. Lett.* **2021**, *775*, 138660.
(41) Raja, A.; Rajasekaran, P.; Selvakumar, K.; Arunpandian, M.; Kaviyarasu, K.; Asath Bahadur, S.; Swaminathan, M. Visible Active Reduced Graphene Oxide-$BiVO_4$-ZnO Ternary Photocatalyst for Efficient Removal of Ciprofloxacin. *Sep. Purif. Technol.* **2020**, *233*, 115996.
(42) Mohamed, N. A.; Safaei, J.; Ismail, A. F.; Khalid, M. N.; Mohd Jailani, M. F. A.; Noh, M. F. M.; Arzaee, N. A.; Zhou, D.; Sagu, J. S.; Teridi, M. A. M. Boosting Photocatalytic Activities of $BiVO_4$ by Creation of G-C_3N_4/ZnO@$BiVO_4$ Heterojunction. *Mater. Res. Bull.* **2020**, *125*, 110779.
(43) Kumar, E. T. D.; Thirumalai, K.; Balachandran, S.; Aravindhan, R.; Swaminathan, M.; Raghava Rao, J. Solar Light Driven Degradation of Post Tanning Water at Heterostructured $BiVO_4$-ZnO Mixed Oxide Catalyst Interface. *Surf. Interfaces* **2017**, *8*, 147−153.
(44) Kim, M. W.; Kim, K.; Ohm, T. Y.; Yoon, H.; Joshi, B.; Samuel, E.; Swihart, M. T.; Choi, S. K.; Park, H.; Yoon, S. S. Electrosprayed $BiVO_4$ Nanopillars Coated with Atomic-Layer-Deposited ZnO/TiO_2 as Highly Efficient Photoanodes for Solar Water Splitting. *J. Chem. Eng.* **2018**, *333*, 721−729.
(45) Hou, H.; Liu, H.; Gao, F.; Shang, M.; Wang, L.; Xu, L.; Wong, W. Y.; Yang, W. Packaging $BiVO_4$ Nanoparticles in ZnO Microbelts for Efficient Photoelectrochemical Hydrogen Production. *Electrochim. Acta* **2018**, *283*, 497−508.
(46) Peng, F.; Ni, Y.; Zhou, Q.; Kou, J.; Lu, C.; Xu, Z. Construction of ZnO Nanosheet Arrays within $BiVO_4$ particles on a Conductive Magnetically Driven Cilia Film with Enhanced Visible Photocatalytic Activity. *J. Alloys Compd.* **2017**, *690*, 953−960.
(47) Chang, J. S.; Phuan, Y. W.; Chong, M. N.; Ocon, J. D. Exploration of a Novel Type II 1D-ZnO Nanorods/$BiVO_4$ Heterojunction Photocatalyst for Water Depollution. *J. Ind. Eng. Chem.* **2020**, *83*, 303−314.
(48) Hu, C.; Tian, M.; Wu, L.; Chen, L. Enhanced Photocatalytic Degradation of Paraben Preservative over Designed G-C_3N_4/$BiVO_4$ S-Scheme System and Toxicity Assessment. *Ecotoxicol. Environ. Saf.* **2022**, *231*, 113175.
(49) Kansaard, T.; Ishihara, K. N.; Pecharapa, W. Structural, Optical and Photo-Induced Catalytic Properties of Derived-Leucoxene /$BiVO_4$ Composite Prepared by Sonochemical Process. *Optik* **2022**, *267*, 169665.
(50) Li, Y.-l.; Liu, Y.; Hao, Y.-j.; Wang, X.-j.; Liu, R.-h.; Li, F.-t. Fabrication of Core-Shell $BiVO_4$@Fe_2O_3 Heterojunctions for Realizing Photocatalytic Hydrogen Evolution via Conduction Band Elevation. *Mater. Des.* **2020**, *187*, 108379.
(51) Ullah, S.; Fayeza; Khan, A. A.; Jan, A.; Aain, S. Q.; Neto, E. P. F.; Serge-Correales, Y. E.; Parveen, R.; Wender, H.; Rodrigues-Filho, U. P.; Ribeiro, S. J. L. Enhanced Photoactivity of $BiVO_4$/Ag/Ag_2O Z-Scheme Photocatalyst for Efficient Environmental Remediation under Natural Sunlight and Low-Cost LED Illumination. *Colloids Surf., A* **2020**, *600*, 124946.
(52) Lin, Y.; Pan, D.; Luo, H. Hollow Direct Z−Scheme CdS/$BiVO_4$ Composite with Boosted Photocatalytic Performance for RhB Degradation and Hydrogen Production. *Mater. Sci. Semicond. Process.* **2021**, *121*, 105453.
(53) Tang, Q. Y.; Luo, X. L.; Yang, S. Y.; Xu, Y. H. Novel Z-Scheme In_2S_3/$BiVO_4$ Composites with Improved Visible-Light Photocatalytic Performance and Stability for Glyphosate Degradation. *Sep. Purif. Technol.* **2020**, *248*, 117039.
(54) Wang, S.; Zhao, L.; Gao, L.; Yang, D.; Wen, S.; Huang, W.; Sun, Z.; Guo, J.; Jiang, X.; Lu, C. Fabrication of Ternary Dual Z-

https://doi.org/10.1021/acsomega.2c07020
ACS Omega 2023, 8, 4835−4852

Scheme AgI/$ZnIn_2S_4$/$BiVO_4$ Heterojunction Photocatalyst with Enhanced Photocatalytic Degradation of Tetracycline under Visible Light. *Arabian J. Chem.* **2022**, *15*, 104159.
(55) Wang, T.; Cai, J.; Zheng, J.; Fang, K.; Hussain, I.; Husein, D. Z. Facile Synthesis of Activated Biochar/$BiVO_4$ Heterojunction Photocatalyst to Enhance Visible Light Efficient Degradation for Dye and Antibiotics: Applications and Mechanisms. *J. Mater. Res. Technol.* **2022**, *19*, 5017−5036.
(56) Zhu, P.; Sun, X.; Zhu, K.; Wang, J.; Bai, J. Preparing Co-Pi/$BiVO_4$ for Effective Degradation of Sulfur-Containing Organics in Wastewater. *Environ. Technol. Innovation* **2022**, *28*, 102928.
(57) Li, Y.; Xiao, X.; Ye, Z. Facile Fabrication of Tetragonal Scheelite (t-s) $BiVO_4$/g-C_3N_4 Composites with Enhanced Photocatalytic Performance. *Ceram. Int.* **2018**, *44*, 7067−7076.
(58) Pirhashemi, M.; Habibi-Yangjeh, A. Ultrasonic-Assisted Preparation of Plasmonic ZnO/Ag/Ag_2WO_4 Nanocomposites with High Visible-Light Photocatalytic Performance for Degradation of Organic Pollutants. *J. Colloid Interface Sci.* **2017**, *491*, 216−229.
(59) Liu, W.; Liang, B.; Ma, Y.; Liu, Y.; Zhu, A.; Tan, P.; Xiong, X.; Pan, J. Well-Organized Migration of Electrons for Enhanced Hydrogen Evolution: Integration of 2D MoS_2 Nanosheets with Plasmonic Photocatalyst by a Facile Ultrasonic Chemical Method. *J. Colloid Interface Sci.* **2017**, *508*, 559−566.
(60) Aguilera-Ruiz, E.; Zambrano-Robledo, P.; Vazquez-Arenas, J.; Cruz-Ortiz, B.; Peral, J.; García-Pérez, U. M. Photoactivity of Nanostructured Spheres of $BiVO_4$ Synthesized by Ultrasonic Spray Pyrolysis at Low Temperature. *Mater. Res. Bull.* **2021**, *143*, 111447.
(61) Yu, Y.; Yao, B.; He, Y.; Cao, B.; Ren, Y.; Sun, Q. Piezo-Enhanced Photodegradation of Organic Pollutants on Ag_3PO_4/ZnO Nanowires Using Visible Light and Ultrasonic. *Appl. Surf. Sci.* **2020**, *528*, 146819.
(62) Qin, H.; Wang, K.; Jiang, L.; Li, J.; Wu, X.; Zhang, G. Ultrasonic-Assisted Fabrication of a Direct Z-Scheme BiOI/Bi_2O_4 Heterojunction with Superior Visible Light-Responsive Photocatalytic Performance. *J. Alloys Compd.* **2020**, *821*, 153417.
(63) Phadtare, V. D.; Parale, V. G.; Kim, T.; Lee, K. Y.; Kadam, A. N.; Choi, H.; Kim, Y.; Dhavale, R. P.; Lee, S. W.; Park, H. H. Ultrasonically Dispersed Ultrathin G-C_3N_4 Nanosheet/$BaBi_2Nb_2O_9$ Heterojunction Photocatalysts for Efficient Photocatalytic Degradation of Organic Pollutant. *J. Alloys Compd.* **2021**, *884*, 161037.
(64) Li, Y.; Chen, H.; Wang, L.; Wu, T.; Wu, Y.; He, Y. $KNbO_3$/ZnO Heterojunction Harvesting Ultrasonic Mechanical Energy and Solar Energy to Efficiently Degrade Methyl Orange. *Ultrason. Sonochem.* **2021**, *78*, 105754.
(65) Kumar, A.; Khosla, A.; Kumar Sharma, S.; Dhiman, P.; Sharma, G.; Gnanasekaran, L.; Naushad, M.; Stadler, F. J. A Review on S-Scheme and Dual S-Scheme Heterojunctions for Photocatalytic Hydrogen Evolution, Water Detoxification and CO_2 Reduction. *Fuel* **2023**, *333*, 126267.
(66) Shawky, A.; Mohamed, R. M. S-Scheme Heterojunctions: Emerging Designed Photocatalysts toward Green Energy and Environmental Remediation Redox Reactions. *J. Environ. Chem. Eng.* **2022**, *10*, 108249.
(67) Xu, Q.; Zhang, L.; Cheng, B.; Fan, J.; Yu, J. S-Scheme Heterojunction Photocatalyst. *Chem* **2020**, *6*, 1543−1559.
(68) Wang, L.; Zhu, B.; Zhang, J.; Ghasemi, J. B.; Mousavi, M.; Yu, J. S-Scheme Heterojunction Photocatalysts for CO_2 Reduction. *Matter* **2022**, *5*, 4187−4211.
(69) Ghazal, N.; Mohamed, S. A.; Hameed, M. F. O.; Obayya, S. S. A.; El Nazer, H. A.; Madkour, M. Surface and Optoelectronic Impacts of ZnO/$BiVO_4$/MWCNT Nanoheterostructure toward Photodegradation of Water Contaminants. *Surf. Interfaces* **2022**, *33*, 102278.
(70) Zhang, L.; Zhang, J.; Yu, H.; Yu, J. Emerging S-Scheme Photocatalyst. *Adv. Mater.* **2022**, *34*, 2107668.
(71) Xu, Q.; Wageh, S.; Al-Ghamdi, A. A.; Li, X. Design Principle of S-Scheme Heterojunction Photocatalyst. *J. Mater. Sci. Nanotechnol.* **2022**, *124*, 171−173.
(72) Chankhanittha, T.; Nanan, S. Hydrothermal Synthesis, Characterization and Enhanced Photocatalytic Performance of ZnO toward Degradation of Organic Azo Dye. *Mater. Lett.* **2018**, *226*, 79−82.
(73) Chankhanittha, T.; Watcharakitti, J.; Nanan, S. PVP-Assisted Synthesis of Rod-like ZnO Photocatalyst for Photodegradation of Reactive Red (RR141) and Congo Red (CR) Azo Dyes. *J. Mater. Sci.: Mater. Electron.* **2019**, *30*, 17804−17819.
(74) Chankhanittha, T.; Somaudon, V.; Watcharakitti, J.; Piyavarakorn, V.; Nanan, S. Performance of Solvothermally Grown Bi_2MoO_6 Photocatalyst toward Degradation of Organic Azo Dyes and Fluoroquinolone Antibiotics. *Mater. Lett.* **2020**, *258*, 126764.
(75) Chankhanittha, T.; Somaudon, V.; Watcharakitti, J.; Nanan, S. Solar Light-Driven Photocatalyst Based on Bismuth Molybdate (Bi_4MoO_9) for Detoxification of Anionic Azo Dyes in Wastewater. *J. Mater. Sci.: Mater. Electron.* **2021**, *32*, 1977−1991.
(76) Gnanamozhi, P.; Rajivgandhi, G.; Alharbi, N. S.; Kadaikunnan, S.; Khaled, J. M.; Almanaa, T. N.; Pandiyan, V.; Li, W. J. Enhanced Antibacterial and Photocatalytic Degradation of Reactive Red 120 Using Lead Substituted ZnO Nanoparticles Prepared by Ultrasonic-Assisted Co-Precipitation Method. *Ceram. Int.* **2020**, *46*, 19593−19599.
(77) Khan, H. R.; Murtaza, G.; Choudhary, M. A.; Ahmed, Z.; Malik, M. A. Photocatalytic Removal of Carcinogenic Reactive Red S3B Dye by Using ZnO and Cu Doped ZnO Nanoparticles Synthesized by Polyol Method: A Kinetic Study. *J. Sol. Energy* **2018**, *173*, 875−881.
(78) Xue, L.; Liang, E.; Wang, J. Fabrication of Magnetic ZnO/$ZnFe_2O_4$/Diatomite Composites: Improved Photocatalytic Efficiency under Visible Light Irradiation. *J. Mater. Sci.: Mater. Electron.* **2022**, *33*, 1405−1424.
(79) Baral, B.; Mansingh, S.; Reddy, K. H.; Bariki, R.; Parida, K. Architecting a Double Charge-Transfer Dynamics In_2S_3/$BiVO_4$ n-n Isotype Heterojunction for Superior Photocatalytic Oxytetracycline Hydrochloride Degradation and Water Oxidation Reaction: Unveiling the Association of Physicochemical, Electrochemical, and Ph. *ACS Omega* **2020**, *5*, 5270−5284.
(80) Ma, D. K.; Guan, M. L.; Liu, S. S.; Zhang, Y. Q.; Zhang, C. W.; He, Y. X.; Huang, S. M. Controlled Synthesis of Olive-Shaped Bi_2S_3/$BiVO_4$ Microspheres through a Limited Chemical Conversion Route and Enhanced Visible-Light-Responding Photocatalytic Activity. *Dalton Trans.* **2012**, *41*, 5581−5586.
(81) Singh, J.; Kumar, S.; Rishikesh; Manna, A. K.; Soni, R. K. Fabrication of ZnO−TiO_2 Nanohybrids for Rapid Sunlight Driven Photodegradation of Textile Dyes and Antibiotic Residue Molecules. *Opt. Mater.* **2020**, *107*, 110138.
(82) Toloman, D.; Popa, A.; Stan, M.; Stefan, M.; Vlad, G.; Ulinici, S.; Baisan, G.; Silipas, T. D.; Macavei, S.; Leostean, C.; Pruneanu, S.; Pogacean, F.; Suciu, R. C.; Barbu-Tudoran, L.; Pana, O. Visible-Light-Driven Photocatalytic Degradation of Different Organic Pollutants Using Cu Doped ZnO-MWCNT Nanocomposites. *J. Alloys Compd.* **2021**, *866*, 159010.
(83) Wu, J.; Hu, J.; Qian, H.; Li, J.; Yang, R.; Qu, L. NiCo/ZnO/g-C_3N_4 Z-Scheme Heterojunction Nanoparticles with Enhanced Photocatalytic Degradation Oxytetracycline. *Diamond Relat. Mater.* **2022**, *121*, 108738.
(84) Ouyang, K.; Yang, C.; Xu, B.; Wang, H.; Xie, S. Synthesis of Novel Ternary Ag/$BiVO_4$/GO Photocatalyst for Degradation of Oxytetracycline Hydrochloride under Visible Light. *Colloids Surf., A* **2021**, *625*, 126978.

https://doi.org/10.1021/acsomega.2c07020
ACS Omega 2023, 8, 4835−4852